Electroconvection in Suspended Fluid Films

by

Zahir A. Daya

A thesis submitted in conformity with the requirements

for the degree of Master of Science

Department of Physics

University of Toronto

Abstract

A theoretical electrohydrodynamic model is developed to explain the instability of a freely suspended fluid film to electroconvection; an instability that occurs when a sufficiently large potential is applied across it. The instability, which leads to a steady spatially periodic flow pattern comprised of counter-rotating vortices, is found to result from the interaction of the electric field with the surface charge density that develops on the free surfaces. A linear stability analysis of the relevant equations is presented. We define a dimensionless control parameter $\mathcal{R}$, which is proportional to the square of the applied voltage, and find a neutral stability boundary for this parameter as a function of the dimensionless wavenumber κ. The critical values $\mathcal{R}_c$ and κ_c are found from the minimum of the stability curve. From the curvature of the neutral stability boundary at $(\kappa_c, \mathcal{R}_c)$, we calculate the correlation length ξ_0 for the amplitude of the pattern. The linear growth rate $\tau_0{}^{-1}$, which depends on another dimensionless parameter $\mathcal{P}$, is also calculated. ξ_0 and τ_0 are coefficients in the Ginzburg-Landau amplitude equation which describes the weakly nonlinear flow pattern near onset in this system. Results of the analysis are compared with recent experiments on smectic A liquid crystal films.

Acknowledgements

I would like to express my gratitude to my supervisor, Professor Stephen W. Morris, for his interest, insight and input in all aspects of this research. I thank Dr. T. Molteno for thought-provoking conversations during the course of this work. Constructive criticism from Dr. V. Deyirmenjian is acknowledged and appreciated. I thank my colleagues for frequent discussions on a broad range of topics.

Contents

List of Figures

I. INTRODUCTION

Nonlinear, nonequilibrium systems under constant external forcing conditions often have macroscopic spatial structures [1]. These structures are loosely referred to as "patterns". In the words of A. Newell, T. Passot and J. Lega [2],

> "Patterns of an almost periodic nature appear all over the place. One sees them in cloud streets, in sand ripples on flat beaches and desert dunes, in the morphology of plants and animals, in chemically reacting media, in boundary layers, on weather maps, in geological formations, in interacting laser beams in wide gainband lasers, on the surface of thin buckling shells, and in the grid scale instabilities of numerical algorithms."

Whereas patterns appear in an incredibly broad range of physical systems, the rigorous study of patterns is confined to systems for which a detailed microscopic description exists. For this reason, fluid systems are especially good candidates for the study of patterns. In fluid systems, patterns almost always evolve from an unstructured state via an instability.

In this thesis we investigate an electroconvection instability in a freely suspended smectic A liquid crystal film first observed by Morris *et al.* [3–5]. Briefly, the experiment consists of a rectangular film of smectic A that is subjected to a voltage drop. A schematic of the film is shown in Fig. 1. Beyond a well-defined critical voltage drop, the film (which is initially stationary) begins to flow. The flow pattern consists of pairs of vortices bearing strong resemblence to Rayleigh-Bénard convection rolls. The material used was 4-4'-n-octylcyanobiphenyl liquid crystal (8CB) which was lightly doped with tetracyanoquinodimethane (TCNQ). In the smectic phase, the molecules are arranged in layers, each layer consisting of orientationally ordered long molecules. The film is always an integer number of layers thick. Each layer of smectic A 8CB is approximately $3.16nm$ thick. In smectic A, the long axis of the molecules is normal to the layer plane. In this arrangement, smectic A exhibits two dimensional (2D) fluid properties in the layer plane. Flows normal to the layer are prevented. Furthermore, the smectic A is isotropic in the plane, and so behaves as an isotropic 2D fluid

[4]. Faetti *et al.* [6] have previously conducted experiments on nematic liquid crystal films in which they observed a similar pattern forming instability. More recently, this pattern forming instability has been observed in smectic C liquid crystal films [7]. The smectic C phase like the smectic A phase consists of molecules arranged in layers, the long axis of the molecules in smectic C is at a fixed tilt to the normal to the layer, unlike smectic A where the long axis is parallel to the normal to the layer. We emphasize, that even though experiments in freely suspended films have used liquid crystals, the mechanism presented in this thesis is independent of the particular properties of liquid crystals.

The objective of this thesis is to elucidate the mechanism of the instability which results in surface-driven electroconvection in a suspended fluid film. The model we present requires that the flow is 2D, that the fluid is isotropic in 2D and is a weak conductor. The driving process is the electric force that results from the interaction between the electric field and the charge density that resides at the film's free surfaces. Since our system consists of a poorly conducting fluid, we must invariably start with the equations of fluid dynamics and electrodynamics, in fact with the equations of *electrohydrodynamics*. The subject of electro-hydrodynamics (EHD) is concerned with how electrostatic forces alter the fluid velocity of a charged electrically conducting fluid and as a consequence the effects of the restructured fluid velocity on the electric field.

Nonequilibrium spatial patterns can be classified according to the linear instabilities of the detailed nonlinear system [1]. The general classification of patterns are *periodic stationary*, *periodic oscillatory* and *uniform oscillatory*; we elaborate on this classification below. The study of instabilities in fluid dynamics basically asks the question, at what value of a certain parameter or combinations of certain parameters (which will henceforth be referred to as the *control* parameter(s)) does a flow alter? The reason the flow alters is because it is unable to sustain itself against (and hence is unstable to) fluctuations in the flow [8]. Instabilities in fluid systems have been studied extensively, experimentally and theoretically, in several geometries and for several flows. Typical examples include the instabilities of parallel flows between planes (Plane Couette flow and Hagen-Poiseuille

flow [10]), Rayleigh-Bénard convection(RBC) [8], Taylor vortex flow (TVF) [8,10], Bénard-Marangoni convection [11] and electrohydrodynamic convection in nematic liquid crystals [11,12]. There are several methods of investigating the instabilities of fluid flows. The best established of these is linear stability analysis in which one linearizes the governing equations to small (infinitesimal) disturbances to the base state. Then one assumes that the disturbance can be expressed as a linear combination of a basic set of modes. This requires a complete set of functions in which the disturbance can be expanded. It follows that instability to any single mode implies instability of the system [8,13]. Hence identification of the first unstable mode (or the most unstable for a given value of the control parameter) gives the first point of instability. In linear analysis, the geometry and boundary conditions constrain the choice of modes, i.e. they physically constrain the solution. One further assumes that the mode has an exponential time-dependence. Typically the nth mode of the disturbance can be written as

$$A_n(\mathbf{r}, t) = A_n(\mathbf{r})e^{\gamma_n t} \tag{1}$$

where $A_n(\mathbf{r})$ satisfies the boundary conditions and is the nth function of a complete set of functions. If the system is infinite (we restrict ourselves exclusively to this case for the remainder of this thesis) or periodic in at least one spatial dimension, say x in cartesian geometry, then the modes in that dimension are periodic, and may be conveniently expanded in Fourier modes. Eqn. 1 is then replaced by

$$A_n(\mathbf{r}, t) = A_n(y, z)e^{i\kappa_n x + \gamma_n t} \tag{2}$$

The exponential time-dependence implies that if a particular mode is unstable then it grows exponentially. Obviously, this is only true in the region where linearization is valid. The nonlinear terms are important and limit the growth of the mode and hence cause the amplitude of the pattern to saturate. The condition for instability is then that the growth rate γ_n must have a positive real part. Hence, the problem of linear stability analysis, is one of evaluating the growth rate. With the ansatz Eqn. 2 substituted into the linearized equations

(which are by definition first order in the disturbances) results in a eigenvalue problem for the growth rate [8]. In general, the growth rate may be complex and the resulting instability/stability is classified by the sign of the real part of the growth rate and the presence or absence of the imaginary part [1,8]. The flow is stable, if for all modes, the real part of the growth rate is negative. The flow is unstable, if for any mode, the real part is positive. Usually, when an instability occurs, the most unstable mode, the one with the largest real part of the growth rate, is observed. If at the same time, the imaginary part vanishes, then the instability is *stationary* resulting in a *stationary* pattern. If the imaginary part does not vanish, then the instability is *oscillatory* resulting in a *oscillatory* pattern. If it happens that at the instablity the most unstable mode has a non-zero κ_n, then the instability is *periodic* resulting in a *periodic* pattern. On the other hand, if at the instability, a zero Fourier mode occurs then the instability is *uniform* resulting in a new *uniform* non-patterned state. The appropriate combinations of growth rate and Fourier mode result in the three types of patterns referred to earlier; *periodic stationary, periodic oscillatory* and *uniform oscillatory*. When the real part of the growth rate vanishes, the resulting state is called neutrally or marginally stable. The locus of the modes that have vanishing real growth rate, separate the unstable modes from the stable modes. This locus is referred to as the neutral stability boundary. If the vanishing of the real part of the growth rate implies that the imaginary part also vanishes then the neutral solution is stationary and the "principle of exchange of stabilities" is said to hold. It is sometimes difficult to prove or disprove the "principle of exchange of stabilities" [8,9,13] and one often relies on experiment to suggest whether a neutral stationary state exists.

Linear stability analysis identifies the *point of bifurcation*, i.e. the value of the control parameter and the selected mode at which the instability occurs. These parameters are refered to as the *critical* control parameter and the *critical* mode. For pattern-forming instabilities, the critical parameters correspond to a global minimum in the neutral stability boundary at $\kappa \neq 0$. However, linear stability analysis makes no predictions about the nonlinear evolution of the selected mode beyond the critical parameter. There are many approaches to

the nonlinear treatment of the fluid equations, however, the one most directly useful to us, and the only one we discuss, is the amplitude equation approach. It is known that there is much similarity between instabilities in fluid systems and the theory of phase transitions [1,13,14]. The Ginzburg-Landau (GL) amplitude equation, which describes dynamics close to the critical point of a phase transition, also (with the meanings of the variables changed) describes the dynamics near the bifurcation point of many fluid instabilities. By applying a proper perturbation scheme, for example multiple scales expansion, it has been shown for several fluid dynamic systems (for example RBC, TVF) that the full nonlinear set of fluid equations can be reduced to the GL amplitude equation in the weakly nonlinear limit. The GL amplitude equation describes the slow spatial and temporal variation of the bifurcated nonlinear solution just above onset; the pattern. For a one dimensional (1D) periodic stationary pattern forming system, the appropriate GL equation is [1]

$$\tau_0 \frac{\partial A}{\partial t} = \varepsilon A - g|A|^2 A + \xi_0^2 \frac{\partial^2 A}{\partial x^2} . \tag{3}$$

In this equation, ε is the reduced control parameter which is defined in terms of the control parameter $\mathcal{R}$. The reduced control parameter $\varepsilon = (\mathcal{R} - \mathcal{R}_c)/\mathcal{R}_c$ where $\mathcal{R}_c$ is the critical control parameter. τ_0 is the inverse of the linear growth rate, ξ_0 is a correlation length and g is a constant, while A is the slowly varying amplitude of a physical quantity, for instance the velocity of a convecting fluid v, expressed as

$$v \sim A e^{i\kappa_c x}. \tag{4}$$

The linear growth rate and the correlation length can be found from linear stability analysis. The linear growth rate is the growth rate of the critical mode in the limit $\varepsilon \to 0^+$ and the correlation length ξ_0 is a measure of the curvature of the neutral stability boundary at the critical values. One can easily see this from Eqn. 3. The linearization of the GL equation is obtained by setting $g = 0$. For marginal stability, the pattern is stationary, hence we have

$$0 = \varepsilon A + \xi_0^2 \frac{\partial^2 A}{\partial x^2}. \tag{5}$$

If we assume that the amplitude A has a slow spatial dependence $\sim e^{ikx}$, where k is the reduced wavenumber $k = \kappa - \kappa_c$, Eq. 5 gives

$$0 = \varepsilon - \xi_0^2 k^2. \tag{6}$$

Substituting for k and ε gives the neutral stability boundary

$$\mathcal{R}_o(\kappa) = \mathcal{R}_c + \mathcal{R}_c \xi_0^2 (\kappa - \kappa_c)^2. \tag{7}$$

Thus the linear approximation to the time-independent GL equation approximates the neutral stability curve in a Taylor expansion about $(\kappa_c, \mathcal{R}_c)$ up to the quadratic term. By comparison, the correlation length is directly proportional to curvature of the neutral stability boundary $\mathcal{R}_o(\kappa)$ at its minimum. We can investigate the time dependent linearized GL equation by ignoring the spatial variation. We consider

$$\tau_0 \frac{\partial A}{\partial t} = \varepsilon A, \tag{8}$$

which is valid in the limit $\varepsilon \to 0^+$. It follows that the time-dependence of A must vary like $\exp(\varepsilon t / \tau_0)$. This time-dependence reproduces the exponential growth from linear theory, so that τ_0 can be extracted from the linear theory.

Surprisingly, even for complex nonlinear systems, the dynamics of the pattern can be described by theoretically simple equations of *universal* form. The GL equation discussed above is a classic example of this universality. The universality of these equations reflects the *symmetries* of the instability, in fact the amplitude equation describes the *bifurcation* from the base state to the pattern state. Whereas, model amplitude equations (due to their universality) can be used to study patterns in different physical systems, a theoretical exposition must begin with the linear instability of the particular system. For the GL amplitude equation described here, the symmetry of the instability is manifested in the cubic term. It is the first nonlinear term that preserves the symmetry of the equation under a sign change in A and it serves to saturate the growth of A [1]. Different instabilities for different flows with this symmetry have different amplitude equations, but the general

form for a 1D periodic stationary pattern up to the cubic order is as given in Eqn. 3. The physical differences between individual systems is contained in the different coefficients; these coefficients are determined from the microscopic or detailed description of the individual system. The GL equation supports a supercritical bifurcation. It is ubiquitous in physical systems and almost always occur in systems where the instability breaks a symmetry [1,15]. In this case, a translationally invariant system (the unstructured state) is replaced by a periodic pattern which breaks the continuous translational invariance. The bifurcation in the GL equation is described (when $g > 0$) by: when $\varepsilon < 0$, the amplitude $A \equiv 0$. As ε is raised through zero, a non-zero solution to the amplitude A is found. Hence the solution bifurcates at $\varepsilon = 0$ or at $\mathcal{R} = \mathcal{R}_c$. The amplitude A is referred to as an order parameter and the essential criterion is that the order parameter vanishes for $\varepsilon \leq 0$ and is non-zero for $\varepsilon > 0$. The terms "order parameter" are chosen in analogy to the theory of phase transitions. The GL equation that we have discussed (with $g > 0$) describes a continuous, or second order, phase transition.

The remainder of the thesis is organized as follows. In Section 2, we describe the relevant geometry and describe the base state. In Section 3, we outline the governing equations and present a linear stability analysis. In Section 4, we discuss results of the linear stability analysis, compare with experiments by Morris *et al.* [4] and Mao *et al.* [18], and suggest avenues for future work. Section 5 is a short conclusion.

II. THEORETICAL MODEL

A. Overview of previous experimental results

The linear stability analysis that will be developed in the next section has been preceded and motivated by experiments in suspended smectic A films [5,16,17]. In these experiments, the smectic A liquid crystal film spanned a rectangular region approximately $l = 20mm$ long and $d = 2mm$ wide as shown in Fig. 1. The long sides of the film were supported

by tungsten wires of diameter $\sim 20\mu m$. The short sides were supported by glass or plastic wipers that were used to draw the film. The experiments used films of thicknesses, s between ~ 7 and $350nm$. The temperature of the film was between 23° and 25°C. The 8CB liquid crystal has the following phases: solid $\xleftrightarrow{21°C}$ smectic A $\xleftrightarrow{33.5°C}$ nematic $\xleftrightarrow{40.5°C}$ isotropic. It is only in the smectic A phase that the liquid crystal behaves as a 2D fluid. The nematic phase is only partially orientationally ordered and does not display the pronounced layering of the smectic A phase. The flow was visualized by observing the motion of dust or smoke particles in the film with an optical microscope. The experimental procedure for locating the onset of electroconvection was to gradually increase the potential difference, V, across the film and to determine the voltage, V_c at which the film first begins to flow. The potential drop was applied symmetrically, i.e. one of the tungsten electrodes was maintained at $-V/2$ volts while the other at $+V/2$ volts.

The film is observed to undergo a 2D spatially periodic flow consisting of vortices similar to classic thermal convection rolls, when the applied voltage exceeds a well-defined critical threshold, V_c. The pattern is observed to be time stationary and the onset of electroconvection is found to be non-hysteretic. The pattern wavelength at onset, λ_c, is the length of the basic repetitive unit (in this case a pair of rolls). Based on measurements from several film of widths, d, it was found that [17] $\lambda_c{}^{expt} = (1.294 \pm 0.015)d$. The critical voltage was found to increase linearly, for thin films, with film thickness, s, and was approximately independent of the film width, d. Experiments were also performed with an A.C. voltage [5]. For low frequencies (less than one hertz) the vortices are seen to periodically reverse at the applied frequency. The critical voltage increases with increasing frequency. For high frequencies (greater than a few hertz) the convective vortices are relegated to two rows along the electrodes and do not extend into the central region of the film. The wavelength of the pattern is reduced with increasing frequency.

The correlation length, ξ_0, was determined by fitting the amplitude of the measured flow velocity to a solution to the GL amplitude equation. It was found that [18] $\xi_0{}^{expt} = 0.36 \pm 0.02d$. This was accomplished as follows: at a fixed $\epsilon > 0$, and along a line at a

fixed distance and parallel to the electrodes, Mao *et al.* [18] determined the amplitude of the component of the flow velocity parallel to the electrodes as a function of distance from the film edge. The velocity amplitude is pinned to zero (by rigid boundary conditions) at the film's edge and grows to a maximum at the film's center. The amplitude profile so obtained was fit to solution to the time-independent GL equation with $A = 0$ as a boundary condition at the edge of the film (i.e. at $x = 0$) and $A \to A_{max}$ as $x \to \infty$. In this fit, the correlation length is a fitting parameter. The linear growth rate, τ_0, was determined by fitting the measured time evolution of the amplitude of a component of the flow velocity of a film of known thickness (in this case 20 layers) when it was subjected to a sudden change in the applied voltage; it was found that [18] $\tau_0{}^{expt} = 0.505 \pm 0.015$ seconds. The measured time evolution of the amplitude of the flow velocity was fit to a solution of the time-dependent GL equation in which the spatial derivatives are neglected (i.e. the point at which the time evolution of the amplitude was measured was far away from the film's edges and from the electrodes). The boundary conditions for the relevant solution are: for $t < 0$, $\epsilon = 0$ and $A = A_0$, and for $t \geq 0$, $\epsilon > 0$. In the fit, the linear growth rate, $\tau_0{}^{-1}$, is a fitting parameter.

In the next section, we describe the theoretical geometry and state the assumptions that are part of the model we propose.

III. GEOMETRY

Since the experiments (see Fig. 1) have $l/d \gtrsim 10$, we treat the film as an infinitely long strip spanning the region $-\infty < x < \infty, -d/2 \leq y \leq d/2$. Similarly, since $s/d \lesssim 10^{-5}$, we treat the film as a sheet with zero thickness. The theoretical geometry and coordinate system are shown in Fig. 2. We always have the electrode at $y = d/2$ at a voltage $V/2$, while the electrode at $y = -d/2$ is at $-V/2$. Neglecting the film thickness is equivalent to saying that the flow and all other field properties (electric potential, density etc.) *within* the film are 2D, being independent of the z coordinate. The assumption of 2D flow is especially reasonable in the context of smectic A films for reasons noted in the Introduction.

We will assume that the fluid is isotropic in the xy plane and is a poor conductor. Liquid crystals in the smectic A phase have anisotropic conductivities and dielectric permitivities. Since the current is always in the plane of the film, we are interested in the in-plane conductivity (i.e. the conductivity that is perpendicular to the long axis of the liquid crystal molecule). This conductivity for 8CB smectic A is $\sim 10^{-7}(\Omega m)^{-1}$. Typical voltages in electroconvection experiments are around 20 volts. The resulting currents in the film are $\sim 10^{-11}$ amperes. This is a sufficiently small current that we can ignore the effects of the resulting magnetic field. We will for completeness begin our theoretical treatment by including a dielectric permitivity, ϵ, for the film, but we will subsequently show that dielectric polarization effects can be neglected. Since the smectic A has dielectric anisotropy, we note that in our 2D model, only the dielectric permitivity in the plane of the film is required. This is the dielectric permitivity perpendicular to the long axis of the liquid crystal molecules and will hereafter be referred to as $\epsilon_\perp$.

In the experiment, the film's free surfaces are in contact with air at atmospheric pressure. We expect that the flow of the film couples to the air and hence there is some air drag on the film when it is convecting. In the theoretical model we ignore this coupling. The smectic A with the dopant, TCNQ, form a chemical complex whose electrochemistry we neglect. We completely ignore the nature of the charge carriers, their mobilities and all electrode

reactions. We also ignore the diffusion of charge. Due to the film's small mass and heat capacity, its large surface area in contact with the air, it is expected that the film is always in thermal equilibrium with the surrounding air. Viscous and ohmic heating can thus be ignored.

For the film shown in fig 2, we will treat two electrode geometries. The first case, the "wire" case, matches the experiment closely. In this case the electrodes are lines infinitely extended in the x direction and located at $z = 0$ and $y = \pm d/2$. The other case, the "plate" case, consists of electrodes in the form semi-infinite planes, infinitely extended in the x direction, one of which is located at $z = 0$ and $-\infty < y \leq -d/2$, while the other is at $z = 0$ and $d/2 < y \leq \infty$. Experimentally this geometry would be represented by electrodes in the form of wide knife edges. The base state, that is the physical description of the film before the onset of electroconvection, is described for these two electrode geometries in the next section. It will be seen that while the hydrodynamical description is simple, the electrostatic description is quite involved.

A. The Base State

When a voltage $V < V_c$, is applied to the film, there is no fluid motion. Since smectic A is isotropic in the plane and we ignore all z variation in any parameter *within* the film, the current density in the film is constant and uniform. Furthermore, we know experimentally that the material is ohmic, hence the electric field *within* the film is constant and given by $\vec{\mathbf{E}} = -V/d \ \hat{\mathbf{y}}$. Since the in-plane electric field is constant, so is the polarization, $\vec{\mathbf{P}}$. Since the polarization charge density is given by the negative of the divergence of the polarization, $q^{pol} = -\nabla \cdot \vec{\mathbf{P}}$, the base state has a vanishing polarization charge density. It also follows, that since the in-plane electric field is constant, the electric potential decreases linearly from the positive electrode to the negative electrode along the film's surface. From the electric field lines in the yz plane as shown schematically in Fig. 3, it is immediately evident that the component of the electric field normal to the film is discontinuous across each of the film's two free surfaces.

This discontinuity in the z component of the electric field at the film's surface supports a surface charge density there. The charge density builds up on both surfaces, however in the calculation that follows we will solve for the surface charge density on the upper surface of the film. Exploiting the mirror symmetry of the problem in the $z = 0$ plane, we scale the charge density so obtained by a factor of two to account for the lower free surface. In all subsequent calculations that involve the surface charge density, we treat the problem in the upper half space *only*, and use the mirror symmetry to account for the lower free surface. The base state surface charge densities will be explicitly calculated for the two electrode cases in the following subsections. The remaining description of the base state consists of describing the body force field and the pressure distribution. The principal body force is the electrostatic force which is a result of the interaction of the surface charge density and the in-plane electric field. Since the electric field in the base state is a constant, the force is simply proportional to the surface charge density. In principle, given the force field one can calculate the pressure distribution for hydrostatic balance. We do not bother with this

calculation since the pressure term will be eliminated in all subsequent analysis. However, it is easy to show that the pressure is a maximum at the centre of the film ($y = 0$). As expected, all parameters in the base state are independent of x, the coordinate along the film's length. The description so far is qualitative and applies to both electrode geometries. To proceed we calculate the surface charge densities for the two electrode cases.

1. Surface Charge Density for the "wire" case, q_{wire}

In the wire geometry, the potential is specified at the lines $z = 0, y = \pm d/2$ and the z derivative of the potential is zero for $z = 0, |y| > d/2$. Thus, in the upper half of the yz plane, we must solve a mixed boundary value problem for the 2D Laplace equation with Dirichlet conditions for $z = 0, -d/2 \leq y \leq d/2$ and Neumann conditions for $z = 0, |y| > d/2$. For this specific case, the mixed boundary value electrostatic problem may be solved by the theory of dual integral equations [19]. A brief introduction to the method of dual integral equations in the context of this problem is given in the appendix. We must solve for the electric potential, Ψ,

$$\left(\frac{\partial^2}{\partial y^2} + \frac{\partial^2}{\partial z^2} \right) \Psi(y, z) = 0, \tag{9}$$

subject to the mixed boundary conditions

$$\Psi(y, 0) = \frac{V}{d} y \qquad |y| < d/2 \tag{10}$$

$$\frac{\partial \Psi(y, z)}{\partial z} \bigg|_{z=0+} = 0 \qquad |y| > d/2. \tag{11}$$

By separation of variables and using the fact that $\Psi(0, 0) = 0$ when $y = 0$, we make the ansatz that the potential in the upper half plane is given by

$$\Psi(y, z) = \int_0^\infty \frac{A(k)}{k} e^{-kz} \sin (ky) dk. \tag{12}$$

With this ansatz we find the dual integral equations

$$\int_0^\infty \frac{A(k)}{k} \sin (ky) dk = \frac{V}{d} y \qquad |y| < d/2 \tag{13}$$

$$\int_0^\infty A(k) \sin (ky) dk = 0 \qquad |y| > d/2. \tag{14}$$

This pair of integral equations may be solved for the potential in the upper half plane by the method of Sneddon [19], giving

$$\Psi(y,z) = \frac{V}{2} \int_0^\infty \frac{J_1(\frac{kd}{2})}{k} e^{-kz} \sin{(ky)} dk, \tag{15}$$

where J_1 is the first order Bessel function of the first kind. The surface charge density is given by

$$q_{wire}(y) \equiv -2\epsilon_0 \frac{\partial \Psi(y,z)}{\partial z}\bigg|_{z=0^+} = \epsilon_0 V \int_0^\infty J_1(\frac{kd}{2}) \sin{(ky)} dk. \tag{16}$$

In accordance to what we have said earlier, the factor of two in the above equation accounts for the two free surfaces. Eqn. 16 can be evaluated [20] for $|y| < d/2$ giving

$$q_{wire}(y) = \frac{2\epsilon_0 V}{d} \frac{y}{\sqrt{(d/2)^2 - y^2}}. \tag{17}$$

This charge density diverges at the position of the electrodes, which is to be expected. In practice, the finite size of the electrodes (in contrast to the model electrodes of zero radius) eliminates this unphysical divergence [21]. In later sections, it will be seen that the divergence of the charge density is sufficiently weak to be mathematically tractable.

2. Surface Charge Density for the "plate" case, q_{plate}

In the plate electrode geometry, we specify the potential on the whole y axis with $-V/2$ for $y < -d/2$ and $+V/2$ for $y > d/2$. Across the film the potential changes linearly from $-V/2$ to $V/2$. This is then a purely Dirichlet problem for the Laplace equation, 9, which may be solved using a Green function [21,22]. The appropriate Green function is constructed from a unit line charge at (y', z') and its image at $(y', -z')$

$$G(y,z;y',z') = -\log \frac{(y-y')^2 + (z-z')^2}{(y-y')^2 + (z+z')^2}. \tag{18}$$

The potential at any point in the upper half plane is given by

$$\Psi(y,z) = -\frac{1}{4\pi} \int_{-\infty}^\infty \Psi(y',0) \frac{\partial G}{\partial z'}\bigg|_{z'=0} dy' \tag{19}$$

where the derivative of the Green function is with respect to the normal directed *outwards* from the upper half plane. Evaluating this using the Green function Eqn. 18 gives

$$\Psi(y, z) = \frac{z}{\pi} \int_{-\infty}^{\infty} \frac{\Psi(y', 0)}{z^2 + (y - y')^2} dy' \tag{20}$$

in which

$$\begin{aligned}
\Psi(y, 0) \quad &= -\frac{V}{2} & -\infty \geq y \geq -\frac{d}{2} \\
&= \frac{V}{d} y & -\frac{d}{2} < y < \frac{d}{2} \\
&= \frac{V}{2} & \frac{d}{2} \leq y \leq \infty.
\end{aligned} \tag{21}$$

The surface charge density on *both* free surfaces is given by

$$-\frac{\pi}{\epsilon_0} q_{plate}(y) = 2\pi \frac{\partial \Psi(y, z)}{\partial z} \bigg|_{z=0^+} \tag{22}$$

$$= \int_{-\infty}^{-\frac{d}{2}} \frac{-V}{z^2 + (y - y')^2} dy' \bigg|_{z=0^+} + \int_{-\frac{d}{2}}^{\frac{d}{2}} \frac{2Vy'/d}{z^2 + (y - y')^2} dy' \bigg|_{z=0^+} + \int_{\frac{d}{2}}^{\infty} \frac{V}{z^2 + (y - y')^2} dy' \bigg|_{z=0^+}. \tag{23}$$

The last line above results from having interchanged the order of differentiation and integration and using Eqn. 20 and Eqn. 21. After integration, the resulting expression was expanded in power series in z and evaluated at $z = 0$. After some simplification the charge density for the "plate" electrode case is given by

$$q_{plate}(y) = -\frac{2V\epsilon_0}{\pi d} \log \left| \frac{y - d/2}{y + d/2} \right|. \tag{24}$$

Once again, as expected, the charge density diverges where the film and electrode meet. The divergences, as noted earlier, are unphysical and finite size effects of the electrodes would remove the divergences. We nevertheless use both charge densities as derived and the divergences prove to be mathematically tractable. The shape of the surface charge density has significant effects on the theoretical predictions for the onset of electroconvection. The surface charge densities of the two electrode geometries are plotted in Fig. 4.

3. "Charge Inversion" and the Mechanism for Electroconvection

It is evident from Fig. 4, that there is greater positive surface charge density close to the positive electrode and greater negative surface charge density close to the negative electrode. This is also schematically depicted in Fig. 3. We refer to this configuration as *charge inversion* and it is analogous to the unstable "top-heavy" mass density configuration in Rayleigh-Bénard convection. It is easy to see that this configuration is potentially unstable. Consider two parcels of film (of equal area) located at $y = y'$ and $y = y' + \triangle$. Taking the linear dimensions of the parcel as small compared to the film width, we may approximate the average surface charge density of the parcel by the value of the surface charge density at the centre of the parcel. Hence, the surface charge density of the parcels are respectively $q_2(y')$ and $q_2(y' + \triangle)$. Since the in-plane electric field is a constant in the base state, the force per unit area on each of the parcels is simply proportional to the surface charge density of the parcel. Consider the interchange of the two parcels. Then the potential energy of the system is reduced by;

$$q_2(y' + \triangle)\vec{\mathbf{E}} \cdot (-\triangle\hat{\mathbf{y}}) + q_2(y')\vec{\mathbf{E}} \cdot \triangle\hat{\mathbf{y}} \tag{25}$$

In this case $\vec{\mathbf{E}} = -V/d \, \hat{\mathbf{y}}$, reducing Eqn. 25 to

$$\frac{V\triangle}{d}\Big(q_2(y' + \triangle) - q_2(y')\Big) \tag{26}$$

It is clear that this is *always* positive and so the exchange of parcels tends to lower the potential energy of the system, hence this configuration of charge density is potentially unstable. It is also easy to see that in a film which has a surface charge density without an inversion, the exchange of parcels leads to an increase in the potential energy. This criterion for potential instability can be stated more succinctly as $\vec{\mathbf{E}} \cdot \nabla q_2 < 0$ [23]. The stabilizing mechanisms are the conduction of charge density and the dissipation due to viscosity. Hence, the instability occurs when the rate of dissipation of kinetic energy by viscosity can be maintained or superceded by the rate of release of potential energy due to the electric force.

Even though the total charge density vanishes in both electrode cases, it is clear from Fig. 4 that there is more charge separation in the "wire" case. The y derivative of the charge density is greater in the "wire" case than in the "plate" case. Hence, we should expect that the "wire" configuration is potentially more unstable than the "plate"configuration. Our results demonstrate this. In the next section, we describe the equations that govern this electrohydrodynamic system and carry out a linear stability analysis.

IV. LINEAR STABILITY ANALYSIS

A. Governing Equations and the Linearized System

The governing equations are those of electrohydrodynamics (EHD). These consist of the Navier-Stokes equation, mass and charge continuity equations and the appropriate Maxwell Poisson equation. Since we consider two dimensional fluid motion only, the Navier-Stokes equation and mass and charge continuity equations are valid in two dimensions, namely the xy plane. However, the *closure* relation, the Maxwell Poisson equation, relates a surface charge density to the potential on the film, and as noted in earlier sections, the surface charge density is related to the potential in the space exterior to the film, hence, this equation is *three dimensional.*

The fluid velocity $\vec{u}$ is confined to the film plane, with $\vec{u} = u\hat{x} + v\hat{y}$. The film is treated as a two-dimensional conducting dielectric fluid, with areal material parameters $\rho_2 = s\rho$, $\eta_2 = s\eta$, $\sigma_2 = s\sigma$, where s is the film thickness and ρ is the bulk density, η is the bulk molecular viscosity, and σ is the bulk conductivity. (In smectic A films, the viscosity is highly anisotropic; the relevant component to use for η is η_3, the viscosity related to shears within layer planes.) The two-dimensional pressure field is given by $P_2 = sP$. The appropriate dielectric constant is $\epsilon_\perp$, the in-plane dielectric permitivity. The body force in the Navier-Stokes equation is the electrostatic force, which results from the interaction of the in-plane electric field, $\vec{E}_2$ with the charge densities; surface charge density, q_2 and

the polarization charge density, $q_2{}^{pol}$. We have already noted that the polarization charge density vanishes in the base state but this is not the case for the perturbed equations, where the polarization is in general not constant. However, we will show that this charge density and the force terms that subsequently appear can be neglected. The Navier-Stokes equation for 2D motion is

$$\rho_2\left[\frac{\partial \vec{\mathbf{u}}}{\partial t} + (\vec{\mathbf{u}} \cdot \nabla_2)\vec{\mathbf{u}}\right] = -\nabla_2 P_2 + \eta_2 \nabla_2{}^2 \vec{\mathbf{u}} + q_2\vec{\mathbf{E}}_2 + q_2{}^{pol}\vec{\mathbf{E}}_2, \tag{27}$$

where ∇_2 is the two-dimensional gradient operator, $\hat{\mathbf{x}}\partial/\partial x + \hat{\mathbf{y}}\partial/\partial y$. The fluid is assumed to be incompressible, so that the mass continuity equation reduces to

$$\nabla_2 \cdot \vec{\mathbf{u}} = 0. \tag{28}$$

The charge continuity equation in the xy plane is

$$\frac{\partial(q_2 + q_2{}^{pol})}{\partial t} = -\nabla_2 \cdot \vec{\mathbf{J}}_2 = -\nabla_2 \cdot (q_2\vec{\mathbf{u}} + q_2{}^{pol}\vec{\mathbf{u}} + \sigma_2\vec{\mathbf{E}}_2), \tag{29}$$

in which $\vec{\mathbf{J}}_2$ is the two-dimensional current density in the plane of the film, which contains contributions from both conduction $(\sigma_2\vec{\mathbf{E}}_2)$ and convection $(q_2\vec{\mathbf{u}} + q_2{}^{pol}\vec{\mathbf{u}})$. To close the system, we require the Poisson equation that relates the electric fields to the charge densities. In practice however, we do not use the Poisson equation directly, but instead we use the Laplace equation with the assertion that the charges lie on the boundary. We do this by choosing a volume in which the Laplace equation is valid and whose boundary consists, in part, of the film surface and electrodes. In the base state, this was particularly simple (since all variables were independent of the x coordinate), where we chose the upper half yz plane as our volume, with the boundary consisting of the y axis and a semi-circle at infinity. In general, we choose the upper half-space with boundary the xy plane (the film and electrodes are in this plane) and a hemisphere at infinity. Hence we have

$$\nabla^2 \Psi = 0. \tag{30}$$

in the half space $z \geq 0$, where $\Psi(x, y, z)$ is the potential. The surface charge density on the *two* free surfaces is given by

$$q_2(x, y) \equiv -2\epsilon_0 \frac{\partial \Psi(x, y, z)}{\partial z}\bigg|_{z=0^+} \tag{31}$$

The in-plane electric field, $\vec{\mathbf{E}}_2$, is given by

$$\vec{\mathbf{E}}_2 = -\nabla_2 \Psi(x, y, 0) \equiv -\nabla_2 \Psi_2. \tag{32}$$

The 2D polarization, $\vec{\mathbf{P}}_2$, is *always* confined to the film plane and is given by $\vec{\mathbf{P}}_2 = s\epsilon_0 \chi_e \vec{\mathbf{E}}_2$, where χ_e is the electric susceptibility of the smectic which is related to the dielectric permittivity by $\epsilon_\perp = \epsilon_0(1 + \chi_e)$. The 3D polarization charge density is equal to

$$q^{pol} = -\nabla \cdot \vec{\mathbf{P}}. \tag{33}$$

However, keeping in mind that the polarization is entirely 2D, the 2D polarization charge density, q_2^{pol} is given by

$$q_2^{pol} = s\epsilon_0 \chi_e \nabla_2^2 \Psi_2 \tag{34}$$

where we have made use of Eqn. 32. The set of equations 27 - 34, define our system. At this time we specify rigid boundary conditions on the flow at the edges of the film,

$$\vec{\mathbf{u}} \equiv 0 \qquad and \qquad \frac{\partial v}{\partial y} \equiv 0 \qquad at \qquad y = \pm d/2. \tag{35}$$

Expanding the divergence in Eqn. 29, using Eqn. 28, the charge continuity equation becomes

$$\frac{\partial(q_2 + q_2^{pol})}{\partial t} + \vec{\mathbf{u}} \cdot \nabla_2(q_2 + q_2^{pol}) + \sigma_2 \nabla_2 \cdot \vec{\mathbf{E}}_2 = 0. \tag{36}$$

One may be tempted at this stage to equate the 2D divergence of the in-plane electric field to the surface charge density. This is incorrect and we emphasize that whereas a charge density is proportional to the 3D divergence of the electric field, there is no simple in relation for this system between the surface charge density and the 2D divergence of the in-plane electric field. To examine the stability of the base state, we introduce perturbations

$$\vec{\mathbf{u}} = 0 + \vec{\mathbf{u}}^{(1)}, \tag{37}$$

$$q_2 = q_2^{(0)} + q_2^{(1)}, \tag{38}$$

$$q_2{}^{pol} = 0 + q_2{}^{pol\ (1)}, \tag{39}$$

$$P_2 = P_2{}^{(0)} + P_2{}^{(1)}, \tag{40}$$

$$\vec{\mathbf{E}}_2 = \vec{\mathbf{E}}_2^{(0)} + \vec{\mathbf{E}}_2^{(1)}, \tag{41}$$

$$\Psi = \Psi^{(0)} + \Psi^{(1)}, \tag{42}$$

$$\Psi_2 = \Psi_2{}^{(0)} + \Psi_2{}^{(1)}. \tag{43}$$

Several of the above equations are not independent and will be used to simplify the system. In all perturbations the superscript (0) refers to the non-zero base state solution while the superscript (1) refers to the infinitesimal perturbations about the base state. Substituting these perturbations into equations 27 - 36, using some of the properties of the base state and linearizing we get

$$\rho_2 \frac{\partial \vec{\mathbf{u}}^{(1)}}{\partial t} = -\nabla P_2{}^{(1)} + \eta_2 \nabla_2{}^2 \vec{\mathbf{u}}^{(1)} + q_2{}^{(0)} E_x{}^{(1)} \hat{\mathbf{x}}$$
$$+ \left(q_2{}^{(1)} E_y{}^{(0)} + q_2{}^{(0)} E_y{}^{(1)} + q_2{}^{pol\ (1)} E_y{}^{(0)} \right) \hat{\mathbf{y}} \tag{44}$$

$$\nabla_2 \cdot \vec{\mathbf{u}}^{(1)} = 0 \tag{45}$$

$$\frac{\partial}{\partial t} \left(q_2{}^{(1)} + q_2{}^{pol\ (1)} \right) = -\vec{\mathbf{u}}^{(1)} \cdot \nabla_2 q_2{}^{(0)}$$
$$- \sigma_2 \left(\nabla_2 \cdot \left(E_x{}^{(1)} \hat{\mathbf{x}} + E_y{}^{(1)} \hat{\mathbf{y}} \right) \right) \tag{46}$$

$$\nabla^2 \Psi^{(1)} = 0 \tag{47}$$

$$q_2{}^{(1)} = -2\epsilon_0 \left. \frac{\partial \Psi^{(1)}}{\partial z} \right|_{z=0^+} \tag{48}$$

$$\vec{\mathbf{E}}_2^{(1)} = -\nabla_2 \Psi_2{}^{(1)} \tag{49}$$

$$q_2{}^{pol\ (1)} = s\epsilon_0 \chi_e \nabla_2{}^2 \Psi_2{}^{(1)} \tag{50}$$

$$\vec{\mathbf{u}}^{(1)} \equiv 0 \quad and \quad \frac{\partial v^{(1)}}{\partial y} \equiv 0 \quad at \quad y = \pm d/2. \tag{51}$$

It is immediately clear that the convection of polarization charge density is of higher order in perturbed quantities because it disappears from the right hand side of the charge continuity equation, Eqn. 46. We now reduce the system by a series of algebraic manipulations. For brevity, we only state them rather than elaborate the details. We eliminate the pressure field by taking a curl of Eqn. 44. We take a second curl of the resulting equation, use

vector identities and the incompressibility condition to simplify the resulting fourth order differential equation, finally selecting only the $\hat{\mathbf{y}}$ component. We use the properties of the base state solution wherever appropriate in the above set (for example $E_y{}^{(0)} = V/d$ etc.), replace electric fields with the relevant gradients of the potential, eliminate the polarization charge density by replacing it in terms of the potential. This results in the following reduced set of equations:

$$\eta_2 \nabla_2{}^2 \nabla_2{}^2 v^{(1)} - \rho_2 \frac{\partial}{\partial t} \nabla_2{}^2 v^{(1)} - \frac{V}{d} \frac{\partial^2 q_2{}^{(1)}}{\partial x^2} + \frac{\partial q_2{}^{(0)}}{\partial y} \frac{\partial^2 \Psi_2{}^{(1)}}{\partial x^2}$$
$$+ \chi_e s \frac{V \epsilon_0}{d} \frac{\partial^2}{\partial x^2} \nabla_2{}^2 \Psi_2{}^{(1)} = 0, \tag{52}$$

$$\frac{\partial}{\partial t}\left(q_2{}^{(1)} + \chi_e s \epsilon_0 \nabla_2{}^2 \Psi_2{}^{(1)}\right) + v^{(1)} \frac{\partial q_2{}^{(0)}}{\partial y} - \sigma_2 \left(\frac{\partial^2 \Psi_2^{(1)}}{\partial x^2} + \frac{\partial^2 \Psi_2^{(1)}}{\partial y^2}\right) = 0, \tag{53}$$

$$\nabla^2 \Psi^{(1)} = 0$$
$$q_2{}^{(1)} = -2\epsilon_0 \frac{\partial \Psi^{(1)}}{\partial z}\bigg|_{z=0^+} \tag{54}$$
$$\Psi_2^{(1)} = \Psi^{(1)}\big|_{z=0^+}.$$

The above set consists of three equations with three unknowns. The first equation results from the Navier-Stokes equation, the second from the charge continuity equation and the third is the Poisson equation written as the Laplace equation for a charge free volume with charge density only on its bounding surface. At this stage, we emphasize that it is Eqn. 54 that connects Eqns. 52 and 53. This closure, however, has no trivial inversion. For example, the Laplace equation is a difficult 3D mixed boundary value problem in the "wire" case. In the next section, we show that this reduces to a mixed boundary value problem for the Helmholtz equation in 2D. Also note that the polarization charge density plays no part in the coupling between the surface charge density and the potential described by Eqn. 54. The reason for this is that the polarization is *entirely two-dimensional* and is *always* in the film plane. Hence, there does not exist a *surface* polarization charge density but rather a volume polarization charge density which has no z dependence and so can be trivially

converted to the 2D polarization charge density, appropriate for a thin film. The difference between a 2D polarization charge density and a *surface* polarization charge density is that the former is a result of the non-vanishing in-plane divergence of the polarization while the latter requires a discontinuity in the normal component of the polarization. Reiterating, the polarization *always* has vanishing normal component, and so the vanishing of the surface polarization charge density means that there are no further boundary conditions to be applied to Eqn. 54 that originate from the polarization. The linearized set of equations 52 - 54, with physically determined boundary conditions consitute the governing set of equations in our model. In the next section, we choose an appropriate scaling and define relevant dimensionless parameters.

B. Normal Mode expansion and Non-Dimensionalization

Following the procedure discussed in the Introduction, we expand the velocity, charge density and potential perturbations in normal modes which are periodic in x with wavenumber k, and have growth rate γ,

$$v^{(1)} = \Lambda(y)e^{ikx+\gamma t}, \tag{55}$$

$$q^{(1)} = \Theta(y, k, \gamma)e^{ikx+\gamma t}, \tag{56}$$

$$\Psi^{(1)} = \Omega(y, z, k, \gamma)e^{ikx+\gamma t}. \tag{57}$$

After substituting these into equations 52, 53 and 54, we non-dimensionalize the system by dividing lengths by d, times by $\epsilon_0 d/\sigma_2$ and charge densities by $\epsilon_0 V/d$. Let $D = \partial/\partial y$ and define new dimensionless quantities $\kappa = kd$, and $Q(y) = d^2 Dq^{(0)}(y)/\epsilon_0 V$. The choice of non-dimensionalizing the length by d, and the charge density by $\epsilon_0 V/d$ appear naturally from the experimental geometery and the analytic expression for the surface charge density. The time scale is chosen (in retrospect) to conform with the charge relaxation time for a thin sheet [5,16]. This time scale is a factor d/s larger than the charge relaxation time for a bulk medium. The resulting equations (where Λ, Θ and Ω are now understood to be dimensionless) are:

$$(D^2 - \kappa^2)\left(D^2 - \kappa^2 - \frac{\gamma}{\mathcal{P}}\right)\Lambda + \kappa^2 \mathcal{R}\left(\Theta - Q\Omega_2 - \chi_e \frac{s}{d}(D^2 - \kappa^2)\Omega_2\right) = 0, \tag{58}$$

$$(D^2 - \kappa^2)\Omega_2 - Q\Lambda - \gamma\left(\Theta + \chi_e \frac{s}{d}(D^2 - \kappa^2)\Omega_2\right) = 0, \tag{59}$$

$$\left[D^2 + \frac{\partial^2}{\partial z^2} - \kappa^2\right]\Omega = 0,$$

$$\Theta = -2\frac{\partial\Omega}{\partial z}\bigg|_{z=0^+}, \tag{60}$$

$$\Omega_2 = \Omega|_{z=0}.$$

As noted earlier, the ratio of film thickness to width, $s/d \sim 10^{-5}$. This ratio occurs in the Eqns. 58 and 59, in conjunction with terms that originated from the polarization charge

density and the electric force acting on this density. Compared to all other terms in the equations above, the effects of polarization are obviously negligible in the limit of vanishing s/d (and of course finite χ_e). Since for 8CB and other smectic materials $\chi_e \sim 10$, we will henceforth neglect these terms.

The closure relation Eqn. 54 is a 3D Laplace equation with a boundary surface charge density. However, as referred to earlier, the periodic dependence of the potential in the x coordinate reduces this 3D Laplace equation to a 2D Helmholtz equation. Eqn. 60 is the appropriate Helmholtz equation that links Eqn. 58 with Eqn. 59. Since Eqn. 60 is valid in the half plane $x = 0$, $z \geq 0$, which is perpendicular to the plane of the film, it determines the rather complicated nonlocal coupling between the in-plane potential function $\Omega_2(y, \kappa, \gamma) = \Omega(y, 0, \kappa, \gamma)$ and the charge density function $\Theta(y, \kappa, \gamma)$. We emphasize that the *closure* relation which couples the electrodynamics (the charge continuity equation) to the fluid dynamics (the Navier-Stokes equation) is valid in a domain that is orthogonal to the domain in which the fluid equations are valid.

In Eqns. 58 and 59 there are two dimensionless parameters: $\mathcal{R}$, a Rayleigh-like number and $\mathcal{P}$, a Prandtl-like number. In terms of the bulk material parameters, they are given by

$$\mathcal{R} \equiv \frac{\epsilon_0{}^2 V^2}{\sigma \eta s^2}, \tag{61}$$

$$\mathcal{P} \equiv \frac{\epsilon_0 \eta}{\rho \sigma s d}. \tag{62}$$

$\mathcal{R}$, the control parameter, is proportional to V^2. It is interesting to note that $\mathcal{R}$ is independent of d, the width of the film. The Prandtl-like parameter $\mathcal{P}$ may be regarded as the ratio τ_q / τ_v of the two time scales in the problem, the viscous relaxation time $\tau_v = \rho d^2 / \eta$ and the charge relaxation time for thin films [5] $\tau_q = \epsilon_0 d / \sigma s$.

The nonlinear y dependence of the base state charge density $q_2{}^{(0)}(y)$ or equivalently the non-constant slope of the base state charge density $\partial q_2{}^{(0)} / \partial y$, is contained in the non-constant, non-dimensional coefficient $Q(y)$. For the two electrode configurations, "wires" and "plates", we find from Eqns. 17 and 24 that they are given, respectively, by

$$Q_{wire}(y) = \frac{4}{(1 - 4y^2)^{3/2}}, \qquad Q_{plate}(y) = \frac{8}{\pi(1 - 4y^2)}. \tag{63}$$

These are plotted in Fig. 5. The divergences in $Q(y)$ correspond to the unphysical divergences in the base state surface charge densities previously described. Note that $Q_{wire}(y) > Q_{plate}(y)$. In the next section we proceed to search for neutral solutions at the onset of the electroconvective instability.

C. Marginal Stability and Results

We now wish to investigate the stability of the following simplified set of linearized equations, which are valid in the limit $s/d \to 0$;

$$(D^2 - \kappa^2)\left(D^2 - \kappa^2 - \frac{\gamma}{\mathcal{P}}\right)\Lambda + \kappa^2 \mathcal{R}\left(\Theta - Q\Omega_2\right) = 0, \tag{64}$$

$$(D^2 - \kappa^2)\Omega_2 - Q\Lambda - \gamma\Theta = 0, \tag{65}$$

$$\left[D^2 + \frac{\partial^2}{\partial z^2} - \kappa^2\right]\Omega = 0,$$
$$\Theta = -2\frac{\partial\Omega}{\partial z}\bigg|_{z=0^+}, \tag{66}$$
$$\Omega_2 = \Omega|_{z=0} \quad .$$

Stability of the base state corresponds to a real and negative value of the growth rate, γ. Instability of the base state occurs when the growth rate has a real and positive part. Marginal or neutral stability occurs when the growth rate vanishes. At this point the problem reduces to determining the values of the parameters $\mathcal{R}$, $\mathcal{P}$, κ and γ such that non-trivial solutions are permitted by the Eqns. 64, 65 and 66, subject to the boundary conditions (now non-dimensionalized)

$$\Lambda(y = \pm 1/2) = D\Lambda(y = \pm 1/2) = 0. \tag{67}$$

and

$$\Omega_2(y = \pm 1/2) = 0. \tag{68}$$

The latter boundary condition is simply that the potential at the electrodes is fixed and not subject to any perturbations. In searching for marginal solutions, $\gamma = 0$, implies that the problem simplifies to searching for values of $\mathcal{R}$ and κ such that Eqns. 64, 65 and 66 with $\gamma = 0$ have non-trivial solutions that satisfy the boundary conditions Eqns. 67 and 68. When $\gamma = 0$, the dimensionless number $\mathcal{P}$ drops out from the above set of equations. Hence, the

parameter space is significantly reduced when looking for marginal solutions. Since Eqn. 64 consists of a fourth order differential operator acting on the velocity perturbation, Λ, subject to the rigid boundary conditions given by Eqn. 67, we are permitted to assume an expansion for $\Lambda(y)$ in terms of a complete set of orthogonal functions that satisfy the rigid boundary conditions (in this case they are also the eigenfunctions of the fourth order differential operator), viz:

$$\Lambda(y) = \sum_{m=1}^{\infty} A_m C_m(y), \tag{69}$$

where the $C_m(y)$ are even Chandrasekhar functions [8], given by

$$C_m(y) = \frac{\cosh(\lambda_m y)}{\cosh(\lambda_m/2)} - \frac{\cos(\lambda_m y)}{\cos(\lambda_m/2)}. \tag{70}$$

Here λ_m is the mth root of [8] $\tanh(\lambda_m/2) + \tan(\lambda_m/2) = 0$. Only the relative amplitudes of the modes are important in the expansion Eqn. 69. Hence, we set $A_1 \equiv 1$.

The symmetry about $y = 0$ of the variables in the set of Eqns. 64 - 66, the boundary conditions and the occurence of differential operators of even order imply that the solutions are either even or odd. We restrict the expansion to even functions. As in RBC, the expansion in odd functions can be shown to predict a higher onset than the expansion in even ones. The even functions have also been shown to be a good fit to velocity data [5]. Consistent with the velocity perturbation expansion, we expand the potential and charge density perturbations

$$\Omega = \sum_m A_m \Omega_m, \qquad \Theta = \sum_m A_m \Theta_m, \tag{71}$$

where Ω_m and Θ_m are the solutions corresponding to $\Lambda = C_m$ in Eqns. 65 and 66. Further, we denote $\Omega_{2m} = \Omega_m|_{z=0}$. We now procede to solve for Ω_m and Θ_m.

1. The potential function Ω_{2m} for $\gamma = 0$

Substituting C_m for Λ_m in Eqn. 65 with $\gamma = 0$, gives

$$(D^2 - \kappa^2)\Omega_{2m} = QC_m, \tag{72}$$

which may be solved directly by Fourier expansion. Since QC_m is even, we expand in the interval $[-1/2, 1/2]$;

$$QC_m = \sum_{n=0}^{\infty} b_{mn} \cos(2n\pi y), \tag{73}$$

in which

$$b_{m0} = 2 \int_0^{\frac{1}{2}} Q(y)C_m(y)dy, \quad b_{mn} = 4 \int_0^{\frac{1}{2}} Q(y)C_m(y)\cos(2n\pi y)dy. \tag{74}$$

The potential perturbation is also even and for purposes of expansion is periodic with the same interval:

$$\Omega_{2mp}(y) = \sum_{n=0}^{\infty} a_{mn} \cos(2n\pi y) \tag{75}$$

where Ω_{2mp} denotes the particular solution. Then the differential equation above becomes

$$-\sum_{n=0}^{\infty}[(2n\pi)^2 + \kappa^2]a_{mn}\cos(2n\pi y) = \sum_{n=0}^{\infty} b_{mn}\cos(2n\pi y) \tag{76}$$

from which it follows that

$$b_{mn} = -a_{mn}[(2n\pi)^2 + \kappa^2] \tag{77}$$

The general solution is

$$\Omega_{2m}(y) = A(\kappa)\cosh(\kappa y) - \sum_{n=0}^{\infty} \frac{b_{mn}\cos(2n\pi y)}{[(2n\pi)^2 + \kappa^2]} \tag{78}$$

where the first term is the homogenous solution while the second term is the particular solution to Eqn. 72. Imposing the boundary condition Eqn. 68 on the potential perturbation determines $A(\kappa)$, giving for the potential

$$\Omega_{2m} = \sum_{n=0}^{\infty} \frac{b_{mn}}{[(2n\pi)^2 + \kappa^2]}\left(\frac{(-1)^n \cosh(\kappa y)}{\cosh(\kappa/2)} - \cos(2n\pi y)\right). \tag{79}$$

Ω_{2m}, has been calculated using a Romberg numerical* integration scheme [25]. The Romberg integration scheme was used to tabulate the integrals for b_{mn} in Eqn. 74 for the each of the two electrode cases Q_{plate} and Q_{wire}, given by Eqn. 63. We used an upper cutoff of $n = 29$, which was dictated by the double precision accuracy of the Romberg scheme.

2. The charge density function Θ_m for $\gamma = 0$

The surface charge density perturbation that results from the potential perturbation, Ω_{2m} calculated above, amounts to solving the Helmholtz problem specified by Eqn. 66;

$$\left[D^2 + \frac{\partial^2}{\partial z^2} - \kappa^2 \right] \Omega_m(y, z, \kappa) = 0; \quad \Theta_m = -2 \frac{\partial \Omega_m}{\partial z} \bigg|_{z=0^+}. \tag{80}$$

subject to $\Omega_{2m} = \Omega_m(y, 0, \kappa)$ on the film $(-1/2 \leq y \leq 1/2)$. Outside the film along the y-axis $(|y| > 1/2)$ we have for the "wire" case the corresponding Neumann condition that the normal derivative of the potential perturbation vanishes and for the "plate" case the Dirichlet condition $\Omega_{2m} = 0$. The perturbed surface charge density is calculated by first determining the potential in the appropriate half space by a successive overrelaxation scheme (SOR) [25] and then numerically evaluating a one-sided derivative at the film surface. We solved the Helmholtz equation 80 for Ω_m, for each of the two electrode cases, using a simple SOR algorithm. Because Ω_m is even in y, it need only be relaxed in the first quadrant of the yz plane. We used an $N \times N$ square lattice of cells in this quadrant, with $N_{film} < N$ points between $y = 0$ and $y = 1/2$. On the outer edges of the lattice, we set $\Omega_m = 0$ to enforce the zero boundary condition at infinity. Starting with $N = 100$ and $N_{film} = 50$, we systematically increased N and N_{film} is such a way that $N_{film}/N \to 0$. All the quantities calculated below showed a small residual monotonic variation with N_{film}; we removed this by plotting each against $1/N_{film}$ and extrapolating to $1/N_{film} \to 0$. From the resulting Ω_m,

---

*The numerical details for the entire linear stability analysis can be found in ref. [24]. The author is indebted to Professor S.W. Morris for the numerical solution to the linear stability problem.

the charge density perturbation Θ_m was determined from Eqn. 80 by taking the one-sided z derivative numerically. Θ_m was therefore only known at N_{film} lattice points across the film. For the purposes of integration, we used a Chebyshev interpolation [25] of these points.

3. The charge density function Θ_m for $\gamma \neq 0$

The potential function Ω_{2m} and the charge density function Θ_m for $\gamma \neq 0$ are obtained by solving

$$(D^2 - \kappa^2)\Omega_{2m} = QC_m + \gamma\Theta_m \tag{81}$$

by a numerical iterative scheme. We used the $\gamma = 0$ solution Eqn. 79 to find a first approximation $\Omega_{2m}{}^{[0]}$. From this, we calculated the corresponding approximate to the charge density function $\Theta_m{}^{[0]}$ using the relaxation algorithm. Then $QC_m + \gamma\Theta_m{}^{[0]}$ was Fourier expanded in the same manner as QC_m in Eqns. 73 and 74 above. This expansion was used to find a series solution analogous to Eqn. 79 for the next approximation $\Omega_{2m}{}^{[1]}$, which was then relaxed to find $\Theta_m{}^{[1]}$. This sequence of steps was iterated until it converged for both Ω_{2m} and Θ_m. The convergence criterion was a sum of the squares of 100 differences in successive iterates distributed on $0 \leq y \leq 1/2$. For $|\gamma| \leq 0.1$, the sum converged after 7 or 8 iterations to a precision limited by the Romberg integration scheme used to find the Fourier coefficients. In each case, for relaxation, the Dirichlet conditions on Ω_m for $-1/2 \leq y \leq 1/2$ and $z = 0$ are given by $\Omega_{2m}{}^{[j]}$ from the jth order iteration. Beyond the film, for $|y| > 1/2$, $z = 0$, we applied the Dirichlet condition $\Omega_m = 0$ in the plate electrode case, and Neumann conditions $(\partial\Omega_m/\partial z)|_{z=0^+} = 0$ in the wire case.

4. The Compatibility Condition and the Neutral Stability Boundary

To find the general compatibility conditions on solutions, we substitute the expansions for Λ, Ω_2 and Θ into Eqn. 64,

$$\sum_{m=1}^{\infty} \left((D^2 - \kappa^2)\left(D^2 - \kappa^2 - \frac{\gamma}{\mathcal{P}}\right)C_m + \kappa^2 \mathcal{R}\left[\Theta_m - Q\Omega_{2m}\right] \right) A_m = 0. \tag{82}$$

Multiplying by the Chandrasekhar function $C_l(y)$ and integrating from $y = -1/2$ to $y = +1/2$, we form inner products, denoted by $\langle \cdots \rangle$. Then Eqn. 82 becomes a linear homogenous system for the expansion coefficients. For non-trivial solution, we require that the matrix defined by the linear operator (i.e. the inner product on Eqn. 82) should be singular. This is the compatability condition;

$$\left\| \langle C_l(D^2 - \kappa^2)\left(D^2 - \kappa^2 - \frac{\gamma}{\mathcal{P}}\right)C_m \rangle + \kappa^2 \mathcal{R}\langle C_l\left[\Theta_m - Q\Omega_{2m}\right]\rangle \right\| = 0. \tag{83}$$

Using the orthogonality property of the Chandrasekhar functions we get

$$\left\| (\lambda_m^4 + \kappa^4)\delta_{lm} - 2\kappa^2 X_{lm} + \kappa^2 \mathcal{R}F_{lm} - \frac{\gamma}{\mathcal{P}}(X_{lm} - \kappa^2 \delta_{lm}) \right\| = 0, \tag{84}$$

where $F_{lm} = \langle C_l(\Theta_m - Q\Omega_{2m})\rangle$. The matrix elements X_{lm} are given analytically by [8]

$$X_{lm} = \langle C_l'' C_m \rangle \tag{85}$$

$$= \frac{2}{\lambda_l^4 - \lambda_m^4}(C_l''' C_m'' - C_m''' C_l'')\Big|_{y=\frac{1}{2}} \qquad l \neq m \tag{86}$$

$$= \frac{1}{\lambda_m^4}(\frac{1}{2}C_m''' C_m'' - \frac{1}{4}(C_m''')^2)\Big|_{y=\frac{1}{2}} \qquad l = m, \tag{87}$$

where $C_m'' = D^2 C_m(y)$, *etc.* The matrix elements $F_{lm}(\kappa, \gamma)$ were evaluated numerically for each electrode configuration using Romberg integration [25]. The divergences in $Q(y)$ at the edges of the film are overcome because $C_l(y)$ approaches zero faster than either $Q_{wire}(y)$ or $Q_{plate}(y)$ diverges at $y = \pm 1/2$. For the first few Chandrasekhar functions, C_m, the functions Θ_m and Ω_{2m} are simple smooth functions which are straightforward to integrate numerically.

To find the conditions for marginal stability, we set $\gamma = 0$ in the compatibility condition Eqn. 84.[†] The dimensionless group $\mathcal{P}$ drops out, so that the marginal stability conditions

---

[†]Setting $\gamma = 0$ is to assume that the "principle of exchange of stabilities" holds. It is standard procedure to first establish that the growth rate, γ is real before assuming that a marginal state

are independent of the Prandtl-like number, just as is in the Bénard problem. With $\gamma = 0$, and the Prandtl-like number irrelevant, we seek the solution set consisting of the pair $(\kappa, \mathcal{R})$ such that Eqn. 84 holds. Then the locus of this solution set defines the marginal (neutral) stability boundary, $\mathcal{R}_o(\kappa)$ which separates the stable ($\gamma < 0$) from the unstable ($\gamma > 0$) regions in $(\kappa, \mathcal{R})$ space. This locus is evaluated systematically for both electrode geometries. We choose a value of κ, set $l = m = 1$ and calculate $F_{11}(\kappa)$. Then Eqn. 84 can be simply solved to get the first approximation $\mathcal{R}_o^{[1]}(\kappa)$. At the next order, we find $F_{lm}(\kappa)$ for $l, m = 1, 2$ and search near $\mathcal{R}_o^{[1]}(\kappa)$ for roots of the 2×2 determinant 84 to find $\mathcal{R}_o^{[2]}(\kappa)$. We can then use $A_1 = 1$ to find A_2 in Eqn. 69 by backsubstitution. We carried this algorithm to the third order in the Chandrasekhar expansion, for which the maximum of $|A_3| \approx 10^{-2}$ and the resulting neutral curve $\mathcal{R}_o(\kappa)$ no longer changes significantly.

Fig. 6 shows the neutral curve for the two cases of electrode configuration, "wire" and "plates". The minima of these curves define the critical values κ_c and $\mathcal{R}_c = \mathcal{R}_o(\kappa_c)$ for each case. These values are collected in table I.

Fig. 7 shows the amplitudes A_2 and A_3 for the wire case, relative to $A_1 = 1$. It is clear that the higher terms in the Chandrasekhar expansion contribute very little to the sum 69. We can calculate the dimensionless correlation length ξ_0 which appears in the Ginzburg-Landau equation from the curvature of $\mathcal{R}_o(\kappa)$ for κ near κ_c. We define [1,26]

$$\xi_0^2 = \frac{1}{2} \frac{d^2 \varepsilon_c}{d\kappa^2} \bigg|_{\kappa = \kappa_c}, \tag{88}$$

where $\varepsilon_c = (\mathcal{R}_o(\kappa)/\mathcal{R}_c) - 1$. To find ξ_0 accurately, we fit ε_c to a parabola over a range $\kappa = \kappa_c \pm \Delta\kappa$ and then systematically reduced $\Delta\kappa$ until the value of ξ_0 taken from the fit became independent of $\Delta\kappa$. This corresponded to a fitting range such that $\varepsilon_c \leq 5 \times 10^{-4}$. The values of ξ_0 are given in table I. There is a slight dependence of the correlation length

---

exists. However, we know from experiment that the system evolves to a stationary roll state. Hence we are justified in ruling out the possibility of a time-dependent solution and simply assuming that the imaginary part of the growth rate vanishes.

on the electrode geometry, i.e. on the base state charge density profile.

5. The Linear Growth Rate γ

Returning to the full compatibility condition Eqn. 84 with $\gamma \neq 0$, we consider the behavior of the growth rate γ of the linear modes near the critical values of $\mathcal{R}$ and κ. Our objective is to calculate the dimensionless time τ_0 in the Ginzburg-Landau equation which sets the scale of the linear growth rate near onset. We define [1,26]

$$\tau_0^{-1} = \left. \frac{\partial \gamma(\varepsilon)}{\partial \varepsilon} \right|_{\kappa = \kappa_c, \varepsilon = 0^+}. \tag{89}$$

The matrix element $F_{lm}(\kappa, \gamma)$ is rather expensive to calculate for $\gamma \neq 0$, because we must use the iteration scheme outlined earlier. It is most computationally efficient to choose a value of γ, fix $\kappa = \kappa_c$, and then solve Eqn. 84 for $\mathcal{R}$. This was done for ten values of γ in the range $-0.1 \leq \gamma \leq +0.1$, using three Chandrasekhar modes. The results depend on the Prandtl-like dimensionless group $\mathcal{P}$. The resulting function $\gamma(\varepsilon)$, where $\varepsilon = (\mathcal{R}/\mathcal{R}_c) - 1$, is very nearly linear in ε with a $\mathcal{P}$-dependent slope and $\gamma(0) = 0$. We determined τ_0 from polynomial fits to $\gamma(\varepsilon)$ for $\mathcal{P} \geq 0.01$. The results are slightly dependent on electrode configuration; they are collected in table II. Values of τ_0 are plotted as a function of $\mathcal{P}$ for "wire" electrodes in Fig. 8. For $\mathcal{P} > 1$, τ_0 becomes nearly independent of $\mathcal{P}$, and tends to a limiting value.

V. DISCUSSION

A. Reduction to Rayleigh-Bénard convection

By an *ad hoc* assumption we can reduce our linearized set of equations into a form that is mathematically equivalent to the Rayleigh-Bénard equations. The assumption is unjustified but is only mentioned here to elucidate the similarities and more important, the *differences* between thermally driven convection and surface electroconvection. If, instead of the Maxwell Poisson equation, the closure relation (or for purposes of comparison, the

equation of state), we introduce the linear relation $\Theta = \beta\Omega_2$, then our system reduces to Rayleigh-Bénard convection. A local and linear relation between the surface potential and the surface charge density implies that in the base state the charge density profile is linear and that its derivative is a constant, hence we replace $Q(y)$ by the constant Q_0. Making these changes to the pair of Eqn. 64 and 65, we get

$$(D^2 - \kappa^2)\left(D^2 - \kappa^2 - \frac{\gamma}{\mathcal{P}}\right)\Lambda + \kappa^2\mathcal{R}\left(\beta - Q_0\right)\Omega_2 = 0, \tag{90}$$

$$(D^2 - \kappa^2 - \gamma\beta)\Omega_2 = Q_0\Lambda. \tag{91}$$

Up to scaling and trivial redefinition of variables this pair is equivalent to the corresponding Rayleigh-Bénard convection equations [8]. The fact that we have a different closure relation or equation of state that relates two of the three variables in the problem makes electroconvection interestingly different from Rayleigh-Bénard convection. This equation of state is implicitly defined by a partial differential equation with its own set of boundary conditions. As we have mentioned there is no simple inversion or integral solution to this partial differential equation, hence we do not have a simple functional equation of state as in Rayleigh-Bénard convection. There is added difficulty in this problem, since the instability results via an inversion of *surface* charge density. The nonlocal interaction of the *surface* charges results in the disconnected spaces or domains of validity for the fluid problem and for the electrostatic problem.

B. Comparison to previous experiments

Eqn. 61, combined with the neutral curve, predicts that the onset of convection occurs at a critical voltage, proportional to the film thickness s, given by

$$V_c = \frac{s}{\epsilon_0}\sqrt{\sigma\eta\mathcal{R}_c}. \tag{92}$$

V_c has been found experimentally to be proportional to s in smectic films [5,17,18]. The linear relation holds well for thin smectic films (2 - 24 smectic layers or 6.32 - 75.84 nm). For larger

thicknesses, V_c grows somewhat more slowly than the predicted linear growth. This is almost certainly a consequence of layer-over-layer shears in the z direction that we have neglected. A linear dependence of V_c on s was also observed in the "vortex mode" in suspended nematic films [6], although these films have relatively large thickness nonuniformities and exhibit slow flows even below the onset of convection making $V_c(s)$ considerably more difficult to measure. The dependence of V_c on $\sqrt{\sigma\eta}$ follows inevitably from dimensional analysis; no experimental data is currently available that might demonstrate this relation. The linear dependence of V_c on $s\sqrt{\sigma\eta}$ is also predicted for the "vortex mode" in nematic films proposed by Faetti, Fronzoni and Rolla [6]. The quantitative comparison between Eqn. 92 and experimental data is reasonable. The material parameters, the conductivity σ and especially the viscosity η are not well known. In experiments by Morris *et al.* [5] the conductivity for the film was measured to be $(6.6 \pm 0.3) \times 10^{-8}(\Omega m)^{-1}$. The viscosity that we use is estimated by extrapolating measurements of η made in the higher temperature nematic phase [29,30]. At 23°C, the temperature at which Morris *et al.* conducted their experiments, the relevant viscosity is 0.045 ± 0.008 kg/ms. The effects of doping the 8CB on viscosity have yet to be investigated. We expect that there is a significant change in the viscosity of the doped sample from the pure sample based on observing that the smectic-nematic phase transition temperature is higher for the doped smectic. Morris *et al.* report that $V_c/s = 0.22 \pm 0.05$ volts/layer, where s is measured in units of the smectic layer thickness. Using the above values for the conductivity and viscosity, and using $\mathcal{R}_c$ for the "wire" case, we find that theory predicts $V_c/s = 0.17 \pm 0.02$ volts/layer, which is consistent with the data. However, later experiments by Mao *et al.* [18] found $V_c/s = 1.05 \pm 0.01$ volts/layer. Using an estimated conductivity of $(2.0 \pm 0.2) \times 10^{-7}(\Omega m)^{-1}$, these data seem to require a value of viscosity much larger than the above extrapolated estimate. Resolution of this discrepancy will have to wait until the conductivity and viscosity can be independently measured in the same sample.

The most recent experiments on smectic films [18] show no dependence of V_c on d for films with d between 0.7 and 2.0 mm, with thicknesses s between 2 and 25 molecular layers,

that is, between 6.3 nm and 80 nm. This is consistent with the prediction of Eqn. 92. Over about the same range of thickness, as noted above, V_c is also proportional to s, as predicted. A weak variation of V_c with d was, however, observed in earlier work [5] for d in the larger range of 0.36 mm to 3.5 mm. This work used a thicker film (107 molecular layers, or 340 nm) and a slightly different electrode configuration, with guard electrodes outside the main electrode wires. These features may have contributed some d-dependent three-dimensional effects. Finite size effects of the electrode wires must certainly become significant for small d. The dependence on d observed, shown in Fig. 2 of Ref. [5] is strongest for small d, and tends to decrease for larger d, as one would expect from finite electrode size effects. In suspended nematics [6], it is also observed that V_c increases only weakly with d.

The wavenumber at onset observed in smectic film experiments is [18] $k_c^{expt} = 4.94 \pm 0.03 \ d^{-1}$. The measured value of d is uncertain to $\pm 5\%$, so this result yields a measured dimensionless wavenumber $\kappa_c^{expt} = 4.94 \pm 0.25$. This is in good agreement with the value of $\kappa_c = 4.74$ found from the minimum in the calculated neutral curve for "wire" electrodes. At present, no data is available for comparison to the predictions for the plate electrode geometry. The precise position of the critical parameters $(\kappa_c, \mathcal{R}_c)$ depends on the base state surface charge density (or more directly through the slope of the base state surface charge density, $Q(y)$). Figures 4 and 5 reveal that the "wire" case has a steeper slope in the surface charge density than the "plate" case. As we suggested earlier this should result in the "wire" case having a lower critical voltage than the "plate" case. This is indeed the case (see table I).

There is good experimental evidence [5,18] that the onset of electroconvection in smectic A films is a supercritical bifurcation which can be described by the Ginzburg-Landau equation with $\varepsilon \propto V^2$. The ε dependence of the flow velocity above onset, the behavior of the amplitude of convection near a lateral boundary and the dynamics of changes in the pattern after sudden changes in ε are all well described by fits to Eqn. 3. Our predicted correlation length from the linear stability theory for the "wire" case, $\xi_0 = 0.285$, is about 20% smaller than the experimental value of $\xi_0^{expt} = 0.36 \pm 0.02$. This is in fair, but not completely sat-

isfactory, agreement. Experimentally, determing the correlation length requires the film to be convecting at some measurable velocity. In a convecting film, we expect that the film couples to the air and the effects of air drag may explain the difference between experiment and theory. To arrive at both κ_c^{expt} and ξ_0^{expt}, the experimental measurements were made nondimensional by dividing by the measured film width d, which is known to within about 5%.

All realistic smectic films are sufficiently viscous that they have values of $\mathcal{P} \gg 1$, so that we expect the infinite-$\mathcal{P}$ limiting value of τ_0 to apply. This is easily seen for the rectangular films that experiments have been performed on. Substituting typical values for the film width and thickness, the mass density is approximately 10^3 kg/m^3, and using the values of the conductivity and viscosity given earlier we find

$$\mathcal{P} = \frac{\epsilon_0 \eta}{\rho \sigma s d} \sim 100. \tag{93}$$

The experimental time relaxation parameter is non-dimensionalised using $\tau_q = \epsilon_0 d / \sigma s$. The conductivity σ for doped 8CB has been measured both at 1kHz in a bulk sample [27] and at dc in an annular film [28]; over this frequency range, it changes by a factor of three. This suggests that the conductivity might depend on some frequency dependent electrochemistry and on some surface conductivity. The conductivity appropriate for the theory is the conductivity of the *film*; the conductivity measured *in situ*. Using the dc value, $(3.3 \pm 0.1)^{-7} (\Omega m)^{-1}$, gives a dimensionless experimental τ_0 which is 70% larger than the theoretical value of 0.351, while using the 1kHz value of $(1.11 \pm 0.09) \times 10^{-7} (\Omega m)^{-1}$, gives a dimensionless experimental τ_0 which is 40% smaller than the theoretical value. One must remember that τ_0 is determined experimentally by measuring the time evolution of the velocity field of the film when subjected to a sudden change applied voltage. It is plausible to suggest that this involves a transient time-dependent coupling to the air i.e. the air drag is a function of the velocity of the flow. The differences between the theoretical model and the experiment in this respect may account for some of the difference in predicted and observed values of the linear growth rate.

In general, the agreement between theory and experiment is satisfactory for the quantities κ_c and ξ_0, which scale simply with the width of the film d. However, there is only ambiguous agreement for the quantities V_c/s and τ_0, whose scaling involves the conductivity and/or the viscosity, which are poorly known.

C. The Nonlinear Electroconvection Equations

Having solved the linear problem, we can now return to the original incompressible EHD equations, non-dimensionalize and algebraically manipulate them to suit *any* 2D *film* electroconvection geometry. We emphasize "film" to imply the coupling of the electrostatic force to the hydrodynamic problem through the free surfaces. Then we have for the velocity field, $\vec{u}_2$, the potentials, Ψ_2 and Ψ and the surface charge density, q_2;

$$\left[\nabla_2{}^2 - \frac{1}{\mathcal{P}}\frac{\partial}{\partial t}\right]\left(\nabla_2{}^2\vec{u}_2\right) + \mathcal{R}\left[\nabla_2 \times \left(\nabla_2 q_2 \times \nabla_2\Psi_2\right)\right] = \frac{1}{\mathcal{P}}\left(\vec{u}_2 \cdot \nabla_2\right)\left(\nabla_2{}^2\vec{u}_2\right) \tag{94}$$

$$\frac{\partial q_2}{\partial t} + \vec{u}_2 \cdot \nabla_2 q_2 - \nabla_2{}^2\Psi_2 = 0 \tag{95}$$

$$\begin{aligned}\nabla^2\Psi &= 0, \\ q_2 &= -2\frac{\partial\Psi}{\partial z}\bigg|_{z=0^+}, \\ \Psi\bigg|_{z=0} &= \Psi_2.\end{aligned} \tag{96}$$

These equations hold in any 2D electrode geometry where the film is assumed to lie on the plane $z = 0$. Since we have an incompressible 2D flow, we can in principle replace the velocity field with a stream function, ψ such that $\vec{u}_2 = \nabla \times (0, 0, \psi)$. In the above, the dimensionless parameters $\mathcal{R}$ and $\mathcal{P}$ are

$$\mathcal{R} = \frac{\epsilon_0{}^2 V^2}{\sigma\eta s^2}; \qquad \mathcal{P} = \frac{\epsilon_0\eta}{\rho\sigma s L}, \tag{97}$$

where L is the length scale appropriate to the geometry. In rectangular geometry, we used the film width d. Recent experiments were in the large Prandtl-like number limit, in which

case Eqn. 94 simplifies. This simplification results in the loss of time-dependent terms and intrinsically nonlinear terms from Eqn. 94. Low Prandtl-like number films would make interesting study in the nonlinear regime, however, unless one finds materials with the proper material parameters or one can make films an order of magnitude wider, there is little hope in reducing the Prandtl-like number and still retaining the validity of EHD.

Furthermore, the limitation to 2D flow means that the breadth of secondary instabilities is limited to those that do not involve changing the vortex axis. Note that vortex stretching is itself impossible in 2D fluid dynamics [31]. The secondary instability that appears in this system is the Eckhaus instability [1,11]. This instability restricts the range of wavenumbers that can appear beyond onset. In experiments, this corresponds to the number of vortices. Vortex pairs can be added or removed as a function of the applied voltage beyond the critical voltage. As such, the Eckhaus instability determines the band of *stable* wavenumbers for the vortex state. In principle we can calculate the Eckhaus boundary. This involves (see [32,33]) carrying out a numerical procedure to determine the nonlinear solution that describes the vortex state. A linear stability analysis about the vortex solution renders the linear system that determines the Eckhaus boundary. However, in systems of finite length, end-effects dominate. End-selection is the mechanism of creation or destruction of vortex pairs from the ends of the film. This selection process further constrains the band of stable wavenumbers [34,35]. The calculation of the end-selection boundary consists of first truncating a multiple scales expansion of the full set of equations to get the appropriate Ginzburg-Landau equation and then solving this equation with relevant boundary conditions [34]. We do not present this here; it is work in progress [36].

It has been found experimentally that when the film is subjected to potential drops large compared to the critical voltage, the flow becomes unsteady [16]. With the exception of wavenumber selection instabilities and unsteady flow, no other secondary instabilities have been observed. This suggests that the system has a relatively *clean* transition to unsteady flow. The state of unsteady flow has yet to be investigated, however in a 2D model, the lack of vortex stretching implies that the flow may become *2D turbulent* [37,38].

VI. FUTURE WORK

Annular films of smectic A 8CB also exhibit electroconvection [16]. An annular film is shown schematically in Fig. 9. We intend to study experimentally and theoretically the electroconvection instability in annular films. Electroconvection in annular films allow for the study of hydrodynamic instabilities with a radial force term. There are few experimental systems in which this is possible. RBC is obviously ruled out since the bouyancy force has a directional preference (due to gravity) which cannot be altered on the laboratory scale. Importantly, annular electroconvection is intrinsically non-axisymmetric. Most experiments and theory in annular (or concentric cyclinder) geometry consider axisymmetric instabilities [9,39,40]. We refer mainly to Taylor vortices in Taylor-Couette flow which are axisymmetric. The second bifurcation in Taylor-Couette flow is non-axisymmetric [9,39]. The first bifurcation however, in annular electroconvection is non-axisymmetric. There are other systems where the first bifurcation is non-axisymmetric, for instance Taylor-Couette flow with counter-rotating cylinders [39–41], however, most of them are 3D systems, annular electroconvection in a film is 2D.

Experimentally the differences between annular and rectangular films are significant. The rectangular film has ends and is subjected to end-effects [35], whereas the annular film is free of end-effects. Leak-currents are significant in a rectangular film due to the excess liquid crystal at the edges but are virtually non-existant in an annular film. Experimentally, the annular geometry permits plenty of interesting variations. It is easy to alter the hydrodynamic base state of the film by imposing a shear, by rotating the inner electrode of the annulus. The resulting 2D Couette flow is known to be linearly stable [10]. However, with annular electroconvection we can study the effects of a Couette base state on the electroconvection instability. The other variation in annular geometry that we consider is the eccentric annulus, in which the inner electrode is off-centre. In such a geometry the fluid and electrodynamics is further complicated by non-trivial azimuthal dependencies. It is our intention to study the effects of these symmetry breaking processes on electroconvection in

the annular geometry; by physically changing the geometry to an eccentric annulus (this breaks the inherent azimuthal symmetry in cylindrical geometry), and by altering the base state from a quiescent fluid to that with a shear (this breaks a rotational symmetry and forces a distinction between right and left handedness). Both symmetry breaking processes can also be combined, i.e. the study of electroconvection in an eccentric annular geometry with an imposed shear base state.

Experimentally, we intend to directly measure the current transport through the film. The onset of electroconvection is accompanied by an increase in the current transport i.e. a decrease in the film resistance [5]. This method will allow for a more accurate determination of the onset of electroconvection compared to the visual determination of prior experiments, which required microscopic particles in the flow and the assumption that they behave passively. The behaviour of the convection current as the voltage is varied will be the diagnostic for determining the nature of the bifurcation. Furthermore, the slope of the voltage-current characteristic before the onset of convection gives the resistance and hence the *in situ* conductivity of the annular or eccentric film. The annular geometry can also be made amenable to measure the in-plane viscosity of the smectic film. We intend to do this by setting the inner electrode to a sinusoidal oscillation of known frequency and amplitude. We would then follow particles in the flow and measure the amplitude of their oscillation as a function of their position. Their amplitude is related to the viscosity of the film. The effects of air drag on the viscosity so measured can be accounted for by repeating this experiment as a function of film thickness, the frequency of oscillation of the inner electrode, and using different gases and gas pressures.

Our goal for theoretical work in annular electroconvection, is to predict from the pertinent equations, the points of bifurcation for the various experimental scenarios described earlier. This can be achieved by a linear stability analysis of the system of equations about the base state for the particular scenario. We will follow this with a weakly non-linear analysis to describe the pattern dynamics of the systems and finally we may work towards determining the stability boundaries for secondary instabilities.

VII. SUMMARY AND CONCLUSION

In this thesis, we have proposed a mechanism to explain the electroconvective instability observed by Morris *et al.* [3,5] in freely suspended suspended smectic A liquid crystal films. The mechanism we have proposed is valid for any freely suspended fluid film provided the flow is constrained to move two dimensionally, the fluid is isotropic in 2D and that the fluid is a poor electrical conductor. The pattern forming instability results from the electrostatic force that acts on the charged fluid. As shown in this thesis, the electrostatics require that the fluid carries a surface charge density. In the base state, we have determined that this surface charge density is "inverted" resulting in an unstable configuration. This non-trivial base state charge density is calculated in detail for two electrode geometries.

Relevant governing equations for the theoretical model are explained. A linear stability analysis of the set of equations about the base state is carried out. The complicated, non-local coupling between the surface charge density and the electrostatic force is discussed. Dimensionless parameters appropriate for this system are described: the control parameter, $\mathcal{R}$, and the Prandtl-like parameter, $\mathcal{P}$. Results from the analysis are presented. A neutral stability boundary for the control parameter, $\mathcal{R}$, as a function of the pattern wavenumber, κ is plotted. The onset of the instability (the point of bifurcation) is determined from this curve. The correlation length for the pattern and the linear growth rate are defined and calculated.

Theoretical results are compared with experiments by Morris *et al.* [4,5] and Mao *et al.* [18]. There is good quantitative agreement between the predicted and observed pattern wavelength and pattern correlation length. Theory predicts that the critical voltage varies linearly with the film thickness and is independent of the film width. On both counts, there is qualitative agreement with experiment. A quantitative test of the theory for the critical voltage and the pattern growth rate will require more accurate values of the viscosity and conductivity of smectic A 8CB.

We have proposed future experimental and theoretical work on electroconvection in an-

nular films. In this geometry, we have illustrated the various experimental scenarios that we plan to investigate: a sheared base state and an eccentric annular configuration. We have also described a method to independently determine the viscosity and conductivity of smectic A in the same geometry.

APPENDIX A: MIXED BOUNDARY VALUE POTENTIAL THEORY

In this appendix, we briefly introduce mixed boundary value problems for the Laplace problem. We rely freely on the Sneddon's [19] excellent monogram on this subject. Realistic Laplace problems are often described by the Laplace equation for some potential function subject to mixed boundary conditions. Elliptic partial differential equations with a closed boundary on which are specified either Dirichlet or Neumann conditions are known to have unique solutions [22]. Mixed boundary value problems have the boundary divided into a finite number of subregions with each subregion of the boundary being described by either Dirichlet or Neumann conditions (there must be at least one Dirichlet subregion and one Neumann subregion). For 2D Laplace problems where the boundary consists of two regions, one with Dirichlet boundary conditions and the other with Neumann boundary conditions, the problem is reduced to:

Find a plane harmonic function $\Psi(y, z)$ in the space $z > 0$, which vanishes as $\sqrt{(y^2 + z^2)} \to \infty$ for $z > 0$, and which satisfies the mixed boundary conditions

$$\Psi(y, 0) = F(y), \quad |y| \leq 1; \qquad \left.\frac{\partial \Psi}{\partial z}\right|_{z=0} = 0, \quad |y| > 1, \tag{A1}$$

where $F(y)$ is prescribed.

Note that the domain for the potential is doubly infinite and that the Neumann conditions are homogenous. We will consider two possible solutions depending on the form of the specified function $F(y)$. If $F(y)$ is an even function then an ansatz is

$$\Psi(y, z) = \int_0^\infty k^{-1} A(k) \cos(ky) e^{-kz} dk \tag{A2}$$

Applying the boundary conditions gives the dual pair

$$\int_0^\infty k^{-1} A(k) \cos(ky) dk = F(y) \qquad |y| < 1 \tag{A3}$$

$$\int_0^\infty A(k) \cos(ky) dk = 0 \qquad |y| > 1 \tag{A4}$$

where $F(y)$ is continously differentiable in the interval $|y| < 1$. These and the next pair of dual integrals that we will consider are dual integral equations with trigonometric kernels. We make use of the following cases of the discontinuous Weber-Schafheitlin integral:

$$\int_0^\infty J_1(k) \cos(ky) dk = 1; \qquad\qquad |y| < 1, \tag{A5}$$

$$\int_0^\infty k^{-1} J_1(k) \cos(ky) dk = 0; \qquad\qquad |y| > 1, \tag{A6}$$

$$\int_0^\infty k^{-1} J_{2n}(k) \cos(ky) dk = \frac{1}{2n} \mathcal{F}_n(0, 1/2, y^2); \quad |y| < 1, \tag{A7}$$

$$\int_0^\infty J_{2n}(k) \cos(ky) dk = 0; \qquad\qquad |y| > 1. \tag{A8}$$

In the above, $\mathcal{F}_n$ is the nth Jacobi polynomial. From these, it follows that a solution to dual integral Eqns. A3 and A4 is

$$A(k) = a_0 k J_1(k) + 2 \sum_{n=1}^\infty n a_n J_{2n}(k) \tag{A9}$$

with the constants chosen (having used the orthogonality of the Jacobi polynomials).

$$a_0 = \frac{2}{\pi} \int_0^1 \frac{F(y)}{\sqrt{(1 - y^2)}} dy \tag{A10}$$

$$a_n = \frac{(-1)^n 2^{2-n}}{\Gamma(1/2)\Gamma(n + 1/2)} \int_0^1 \frac{y^{2n}}{(1 - y^2)^{1/2-n}} \left(\frac{1}{y}\frac{\partial}{\partial y}\right)^n F(y) dy \qquad n \geq 1 \tag{A11}$$

The Jacobi polynomials form a complete set of orthogonal functions on the interval $(-1, 1)$. They are defined in terms of the generalized hypergeometric functions [42]:

$$\mathcal{F}_n(a, b, x) =_2 F_1(-n, a + n; b; x) \tag{A12}$$

The constants a_n for the even case are found using the following orthogonality condition

$$\int_0^1 u^{-\frac{1}{2}}(1 - u)^{-\frac{1}{2}} \mathcal{F}_i(0, 1/2, u) \mathcal{F}_j(0, 1/2, u) du = \begin{cases} \frac{1}{2}\pi\delta_{ij} & \text{if} \quad i \neq 0 \\ \pi\delta_{ij} & \text{if} \quad i = 0. \end{cases}$$

On the other hand if $F(y)$ is odd then an ansatz is

$$\Psi(y, z) = \int_0^\infty k^{-1} A(k) \sin(ky) e^{-kz} dk \tag{A13}$$

Boundary conditions render the dual integral equations:

$$\int_0^\infty k^{-1} A(k) \sin(ky) dk = F(y) \quad |y| < 1 \tag{A14}$$

$$\int_0^\infty A(k) \sin(ky) dk = 0 \quad |y| > 1 \tag{A15}$$

The analytic solution to the above pair given by Sneddon is

$$A(k) = \sum_{n=0}^\infty (2n+1) a_n J_{2n+1}(k) \tag{A16}$$

with

$$a_n = \frac{2(-1)^n}{\Gamma(1/2)\Gamma(n+1/2)} \int_0^1 \frac{k^{n+1/2}}{(1-k)^{1/2-n}} \frac{\partial^n}{\partial k^n} \left(\frac{F(\sqrt{k})}{\sqrt{k}} \right) dk \quad n \geq 0 \tag{A17}$$

To illustrate the usage of the above derivations we present the explicit solution for the base state charge density for the "wire" case. We need to solve the Laplace equation in 2D for the electric potential $\Psi(y, z)$;

$$\left(\frac{\partial^2}{\partial y^2} + \frac{\partial^2}{\partial z^2} \right) \Psi(y, z) = 0, \tag{A18}$$

subject to the mixed boundary conditions

$$\Psi(y, 0) = \frac{V}{d} y \quad |y| < d/2 \tag{A19}$$

$$\left. \frac{\partial \Psi(y, z)}{\partial z} \right|_{z=0^+} = 0 \quad |y| > d/2. \tag{A20}$$

For the purposes of this Appendix, we employ a non-dimensionalization where lengths are scaled by half the film width, $d/2$, and potentials by V. This leaves Eqn. A18 unchanged but casts Eqns. A19 and A20 into a form suitable for direct application of the method of dual integrals,

$$\Psi(y, 0) = \frac{y}{2} \quad |y| < 1 \tag{A21}$$

$$\left. \frac{\partial \Psi(y, z)}{\partial z} \right|_{z=0^+} = 0 \quad |y| > 1. \tag{A22}$$

By separation of variables and using the fact that $\Psi(0,0) = 0$ when $y = 0$, we make the ansatz that the potential in the upper half plane is given by

$$\Psi(y,z) = \int_0^\infty \frac{A(k)}{k} e^{-kz} \sin(ky) dk. \tag{A23}$$

With this ansatz we find the dual integral equations

$$\int_0^\infty \frac{A(k)}{k} \sin(ky) dk = \frac{y}{2} \qquad |y| < 1 \tag{A24}$$

$$\int_0^\infty A(k) \sin(ky) dk = 0 \qquad |y| > 1. \tag{A25}$$

This pair of dual integral equations for the Laplace equation has a solution given by Eqn. A16 whose coefficients are given by Eqn. A17. Due to the utter simplicity of the prescribed function $\Psi(y,0) \equiv F(y)$ on the interval $(-1,1)$, the only non-vanishing coeffiecient is a_0;

$$a_0 = \frac{1}{\pi} \int_0^1 \frac{\sqrt{u}}{\sqrt{(1-u)}} du = \frac{1}{2}. \tag{A26}$$

The solution for the dimensionless potential is then

$$\Psi(y,z) = \frac{1}{2} \int_0^\infty \frac{J_1(k)}{k} e^{-kz} \sin(ky) dk. \tag{A27}$$

Reverting to the physically relevant dimensional form, we get

$$\Psi(y,z) = \frac{V}{2} \int_0^\infty \frac{J_1(\frac{kd}{2})}{k} e^{-kz} \sin(ky) dk, \tag{A28}$$

where J_1 is the first order Bessel function of the first kind. This is precisley Eqn. 15 The surface charge density is given by

$$q_{wire}(y) \equiv -2\epsilon_0 \frac{\partial \Psi(y,z)}{\partial z}\bigg|_{z=0^+} = \epsilon_0 V \int_0^\infty J_1(\frac{kd}{2}) \sin(ky) dk, \tag{A29}$$

where the factor of two accounts for the two free surfaces. This integral is analytic and the result, Eqn. 17, is reproduced below:

$$q_{wire}(y) = \frac{2\epsilon_0 V}{d} \frac{y}{\sqrt{(d/2)^2 - y^2}}. \tag{A30}$$

In passing, we make some remarks on other mixed boundary problems. Mixed boundary problems can also be solved in axisymmetric geometry where one sets up dual integrals with

Bessel kernels. Both, dual integrals with Bessel kernels and those with trigonometric kernels, can be solved for non-homogenous Neumann conditions. There are also generalizations to the case when the boundary is divided into three regions resulting in triple integral equations with both the Bessel kernel and the trigonometric kernel. In 2D singly infinite domains (rather than doubly infinite domains) the dual and triple integral equations can be replaced by dual and triple series relations for which there exist some analytic methods.

REFERENCES

[1] M.C. Cross and P.C. Hohenberg, *Rev. Mod. Phys.*, **65**, 851-1112 (1993).

[2] A.C. Newell, T. Passot and J. Lega, *Ann. Rev. Fluid Mech.*, **25**, 399 (1993).

[3] S.W. Morris, J.R. de Bruyn, and A.D. May, *Phys. Rev. Lett.*,**65,**2378 (1990).

[4] S.W. Morris, J.R. de Bruyn, and A.D. May, *J. Stat. Phys.*, **64**, 1025 (1991).

[5] S.W. Morris, J.R. de Bruyn, and A.D. May, *Phys. Rev. A*,**44,**8146 (1991).

[6] S. Faetti, L. Fronzoni and P. Rolla, *J. Chem. Phys.*, **79**, 1427 (1983).

[7] A. Becker, S. Ried, R. Stannarius and H. Stegemeyer, unpublished (1996).

[8] S. Chandrasekhar, *Hydrodynamic and Hydromagnetic Stability*, Dover Publications Inc. (1961).

[9] H.K. Moffat, Six Lectures on General Fluid Dynamics and Two on Hydromagnetic Dynamo Theory, Les Houches, 1973, in *Fluid Dynamics* edited by R. Balian and J.L. Peube, Gordon and Breach Science Publishers (1977).

[10] P.G. Drazin and W.H. Reid, *Hydrodynamic Stability*, Cambridge (1981).

[11] P. Manneville, *Dissipative Structures and Weak Turbulence*, Academic Press Inc. (1990).

[12] L. Kramer and W. Pesch, in *Pattern Formation in Liquid Crystals*, A. Buka and L. Kramer eds. (Springer, New York, 1995).

[13] M.G. Velarde, Hydrodynamic Instabilities (in Isotropic Fluids), Les Houches, 1973, in *Fluid Dynamics* edited by R. Balian and J.L. Peube, Gordon and Breach Science Publishers (1977).

[14] V.M. Zaitsev and M.I. Shliomis, *Soviet Phys. JETP*, **32**, 866 (1971).

[15] P.G. Drazin, *Nonlinear Systems*, Cambridge (1992).

[16] S.W. Morris, Ph.D. Thesis (1991).

[17] S.S. Mao, M.Sc. Thesis (1996).

[18] S.S. Mao, J. R. de Bruyn and S.W. Morris, submitted to *Physica A*.

[19] I. N. Sneddon, *Mixed Boundary Value Problems in Potential Theory*, North-Holland (1966).

[20] I.S. Gradshteyn and I.M. Ryzhik, *Table of Integrals, Series, and Products*, corrected and enlarged edition prepared by A. Jeffrey, Academic Press (1980).

[21] J.D. Jackson, *Classical Electrodynamics*, Wiley (1975).

[22] P.M. Morse and H. Feshbach, *Methods of Theoretical Physics, Part I*, McGraw-Hill (1953).

[23] D.C. Jolly and J.R. Melcher, *Proc. Roy. Soc. Lond. A.*, **314**, 269-283 (1970).

[24] Z. A. Daya, S.W. Morris and J. R. de Bruyn, submitted to *Phys. Rev. E*.

[25] W.H. Press, S.A. Teukolsky, W.T. Vetterling and B.P. Flannery, *Numerical Recipes in C*, Cambridge (1989).

[26] M.A. Dominguez-Lerma, G. Ahlers and D.S. Cannell, *Phys. Fluids*, **27**, 515 (1995).

[27] J.T. Gleeson, private communication.

[28] Z.A. Daya, unpublished (1996).

[29] H. Kneppe, F. Schneider and N.K. Sharma, *Ber. Bunsenges. Phys. Chem.*, **85**, 784 (1981).

[30] S.W. Morris, unpublished (1996).

[31] G.K. Batchelor, *An Introduction to Fluid Dynamics*, Cambridge (1967).

[32] R.M. Clever and F.H. Busse, *J. Fluid Mech.*, **65**, 625 (1974).

[33] H. Riecke and H. Paap, *Phys. Rev. A*, **33**, 547-553 (1986).

[34] M.C. Cross, P.G. Daniels, P.C. Hohenberg, and E.D. Siggia, *Phys. Rev. Lett.*, **45**, 898 (1980); *J. Fluid Mech.*, **127**, 155 (1983).

[35] S.S. Mao, J.R. de Bruyn, Z.A. Daya and S.W. Morris, to be published in *Phys. Rev. E*, 1996.

[36] V. B. Deyirmenjian, Z. A. Daya and S. W. Morris, unpublished.

[37] R.H. Kraichnan and D. Montgomery, *Rep. Prog. Phys.*, **43**, 547-619 (1980).

[38] C.R. Doering and J.D. Gibbon, *Applied Analysis of the Navier-Stokes Equations*, Cambridge (1995).

[39] J.T. Stuart, *Ann. Rev. Fluid Mech.*, **3**, 347-370 (1971).

[40] C.A. Jones, *J. Fluid Mech.*, **102**, 249-261 (1981), **120** 433-450, (1982).

[41] W.F. Langford, R. Tagg, E.J. Kostelich, H.L. Swinney and M.Golubitsky, *Phys. Fluids*, **31**, 776-785 (1988).

[42] M. Abramowitz and I. Stegun, *Handbook of Mathematical Functions*, Dover (1965).
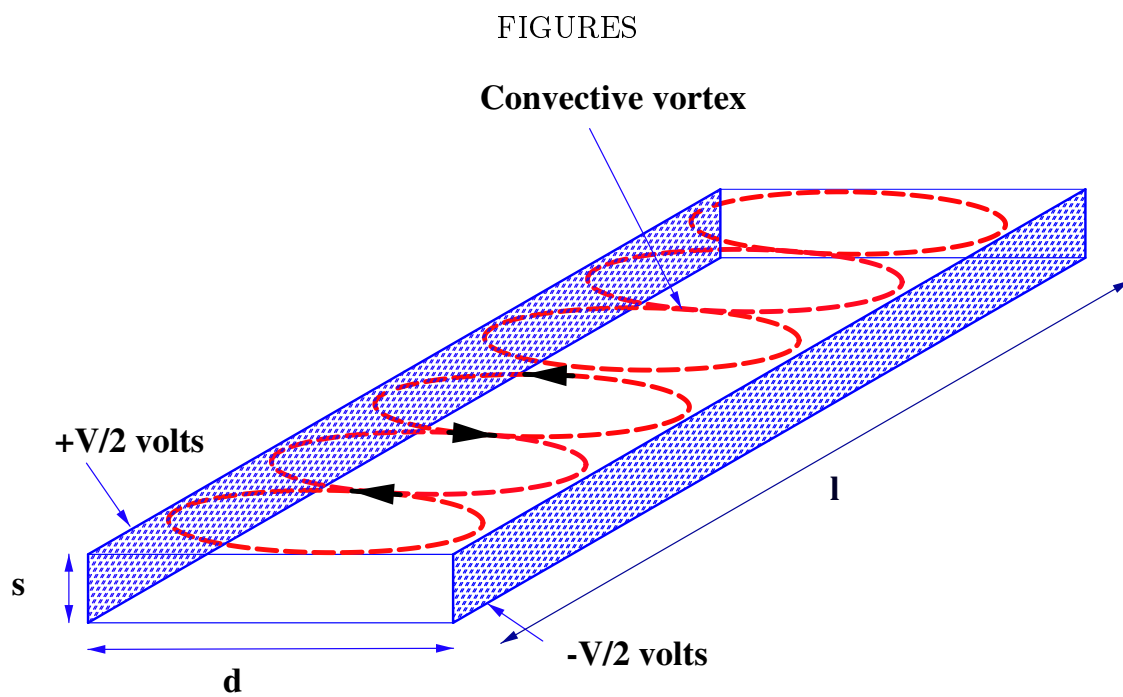
FIG. 1. Electroconvection geometry
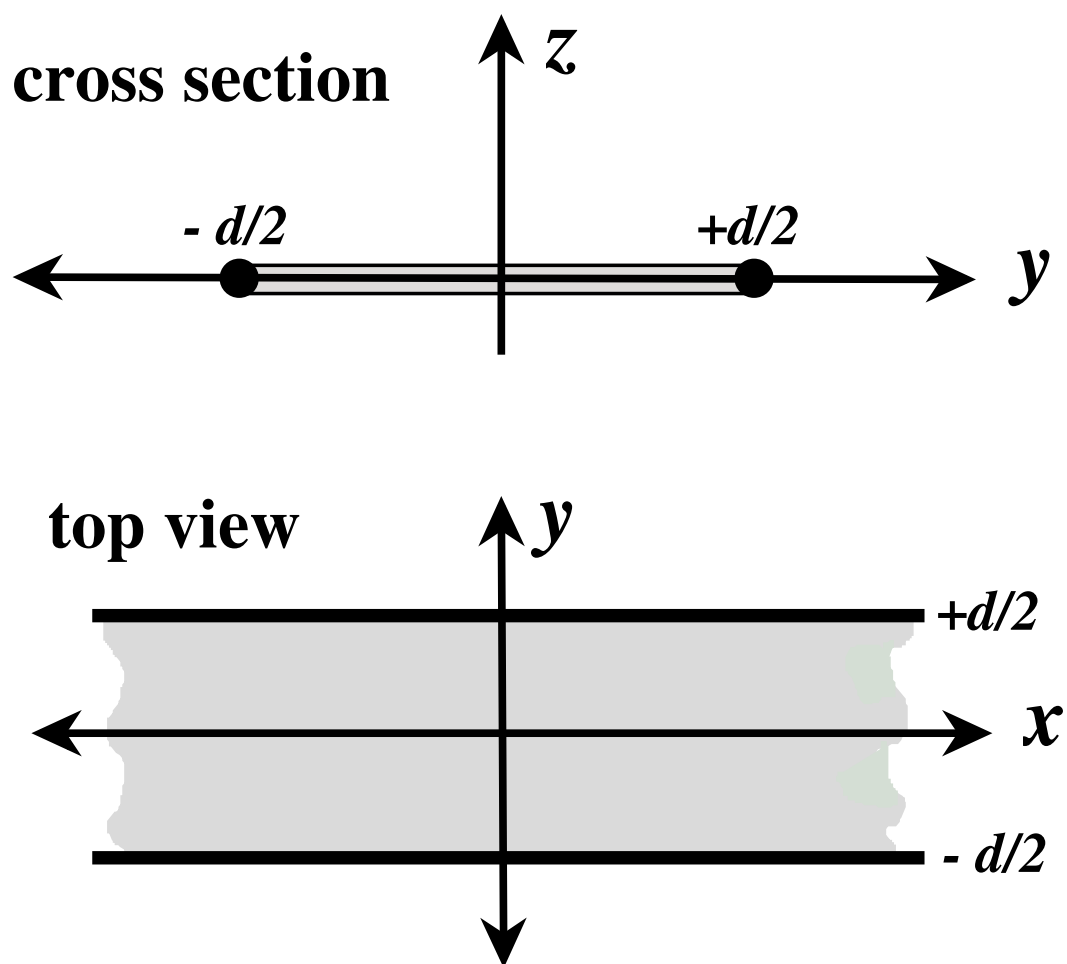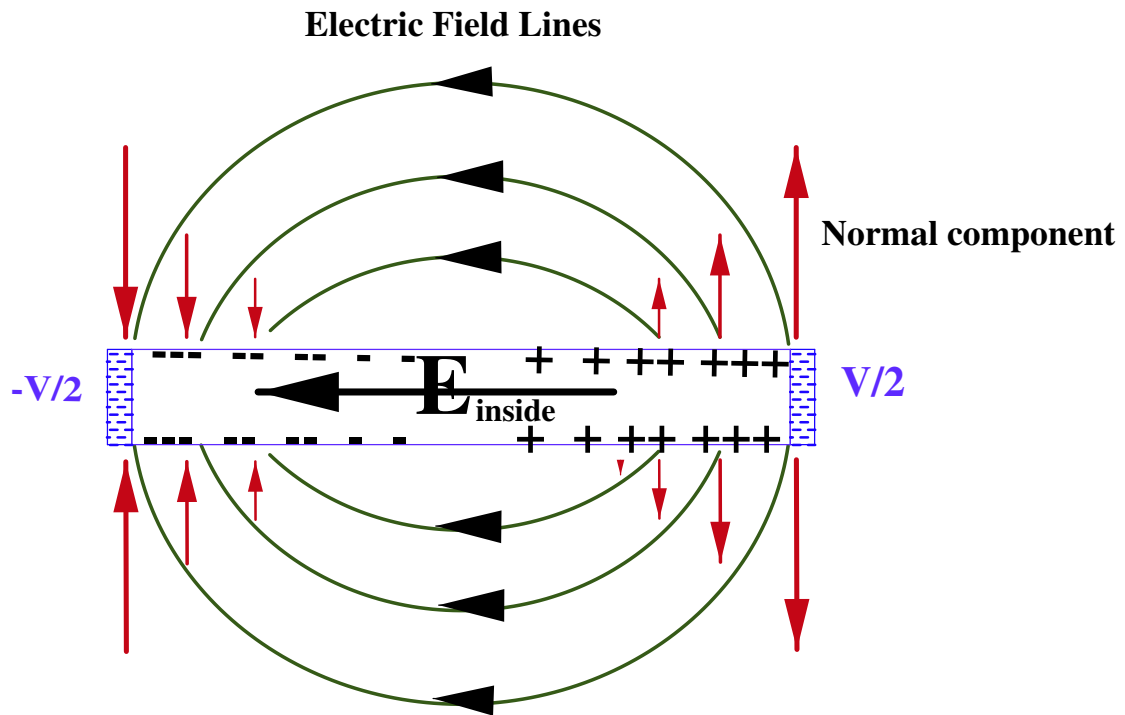
FIG. 2. Coordinates for the theoretical model.

Electric Field Lines

Normal component

-V/2

E_{inside}

V/2

+ + ++ +++

+ + ++ +++

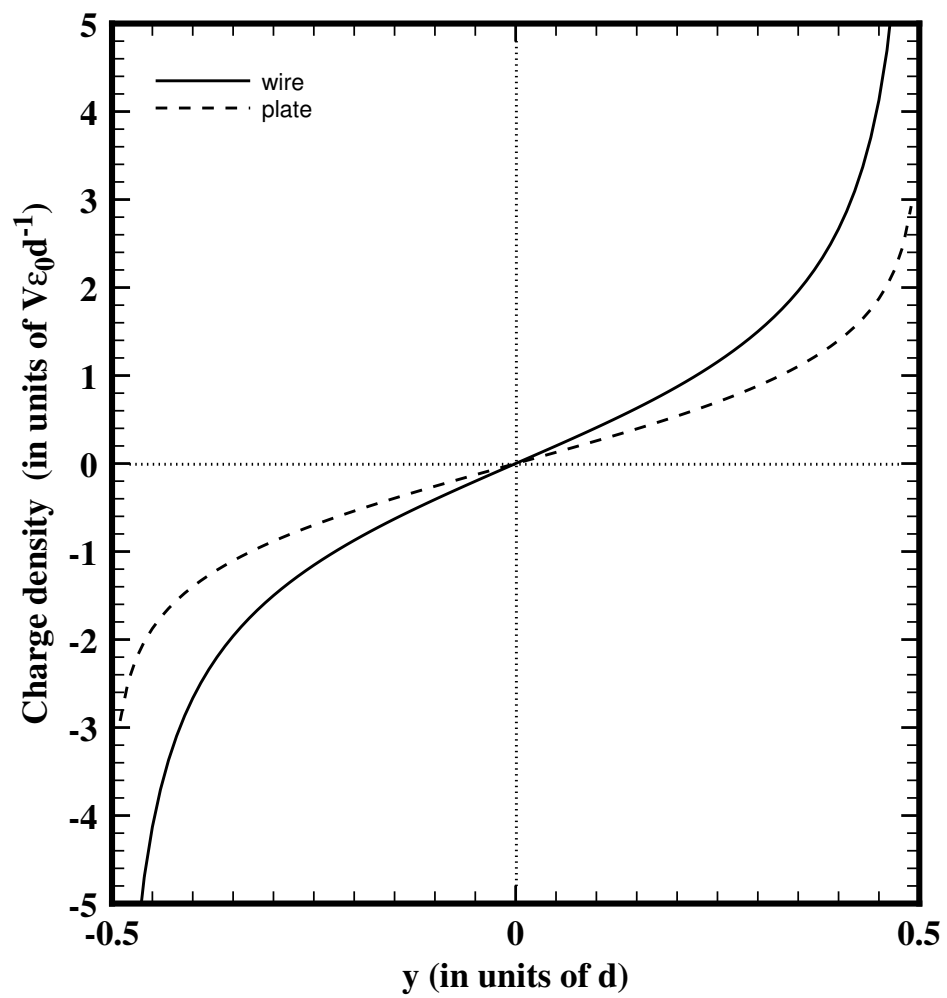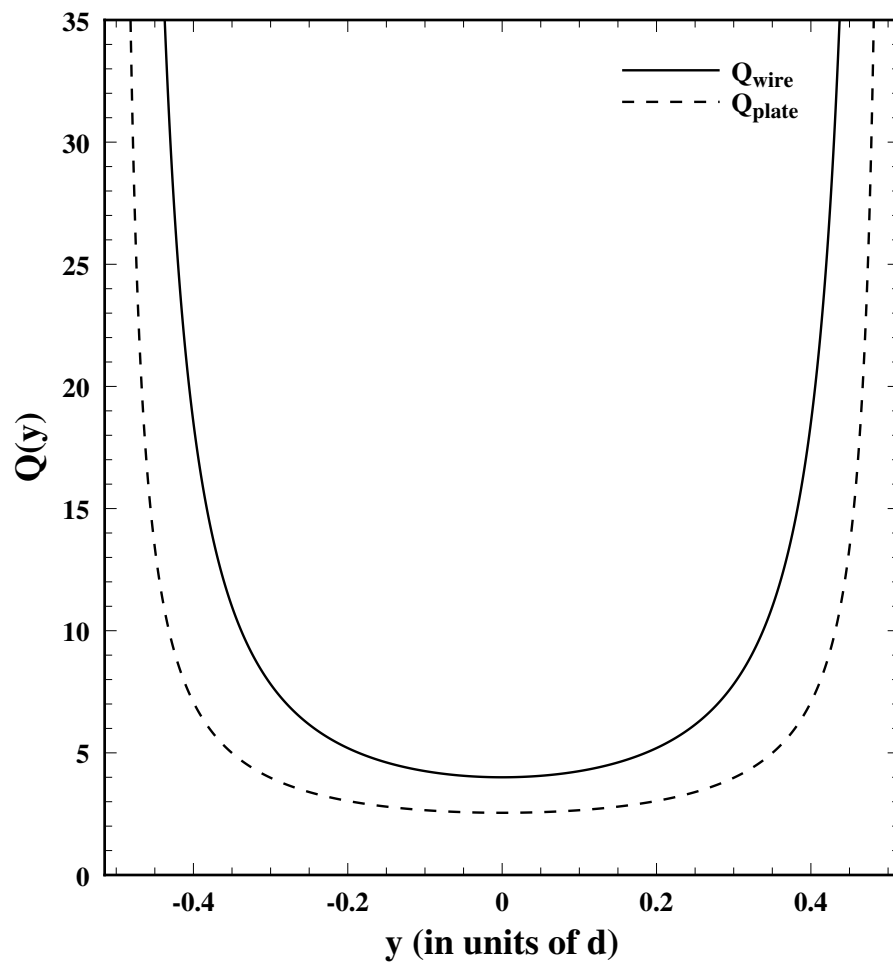FIG. 3. Schematic of Electric Field Lines and Surface Charges

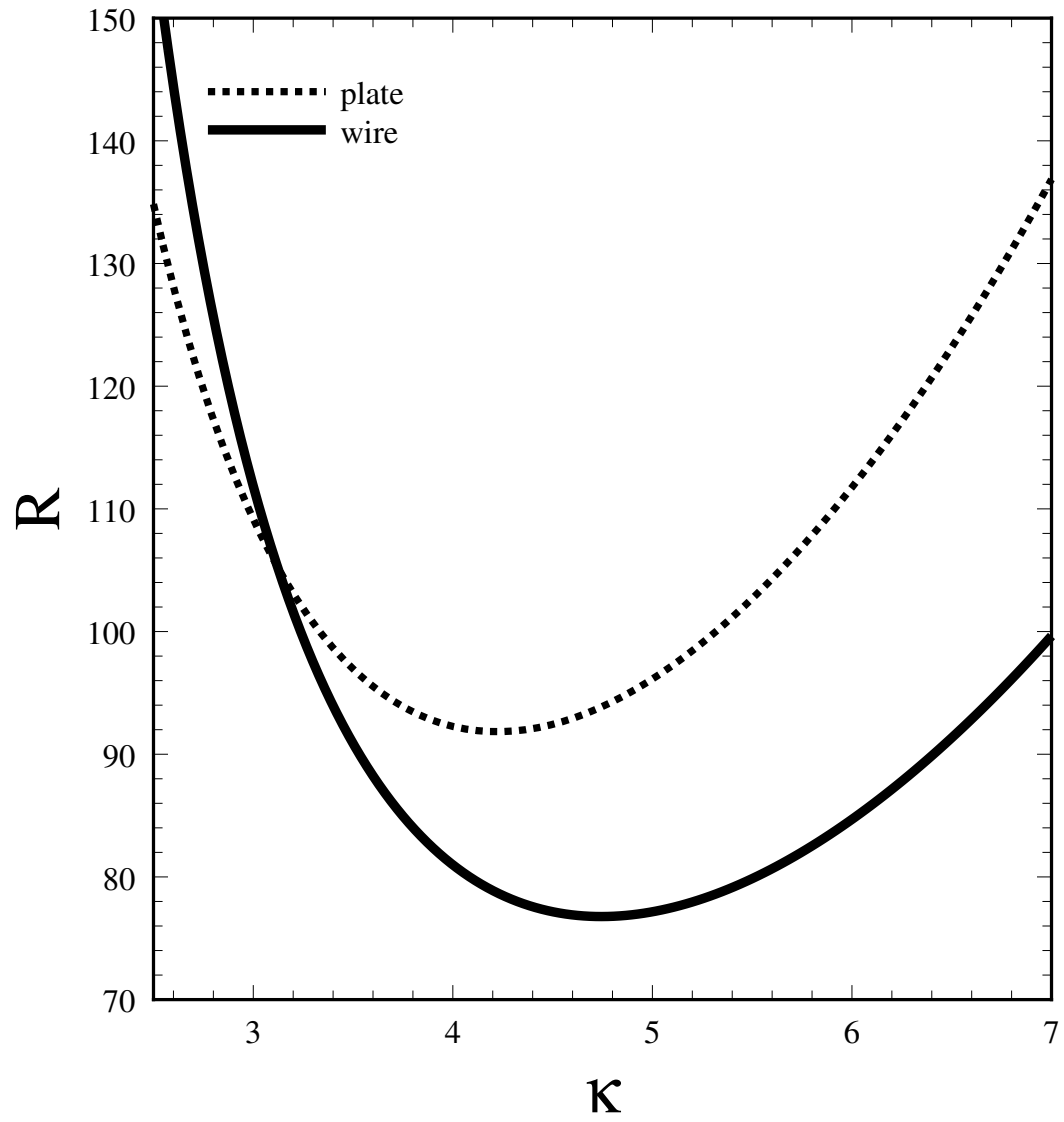FIG. 4. Base State Surface Charge Densities

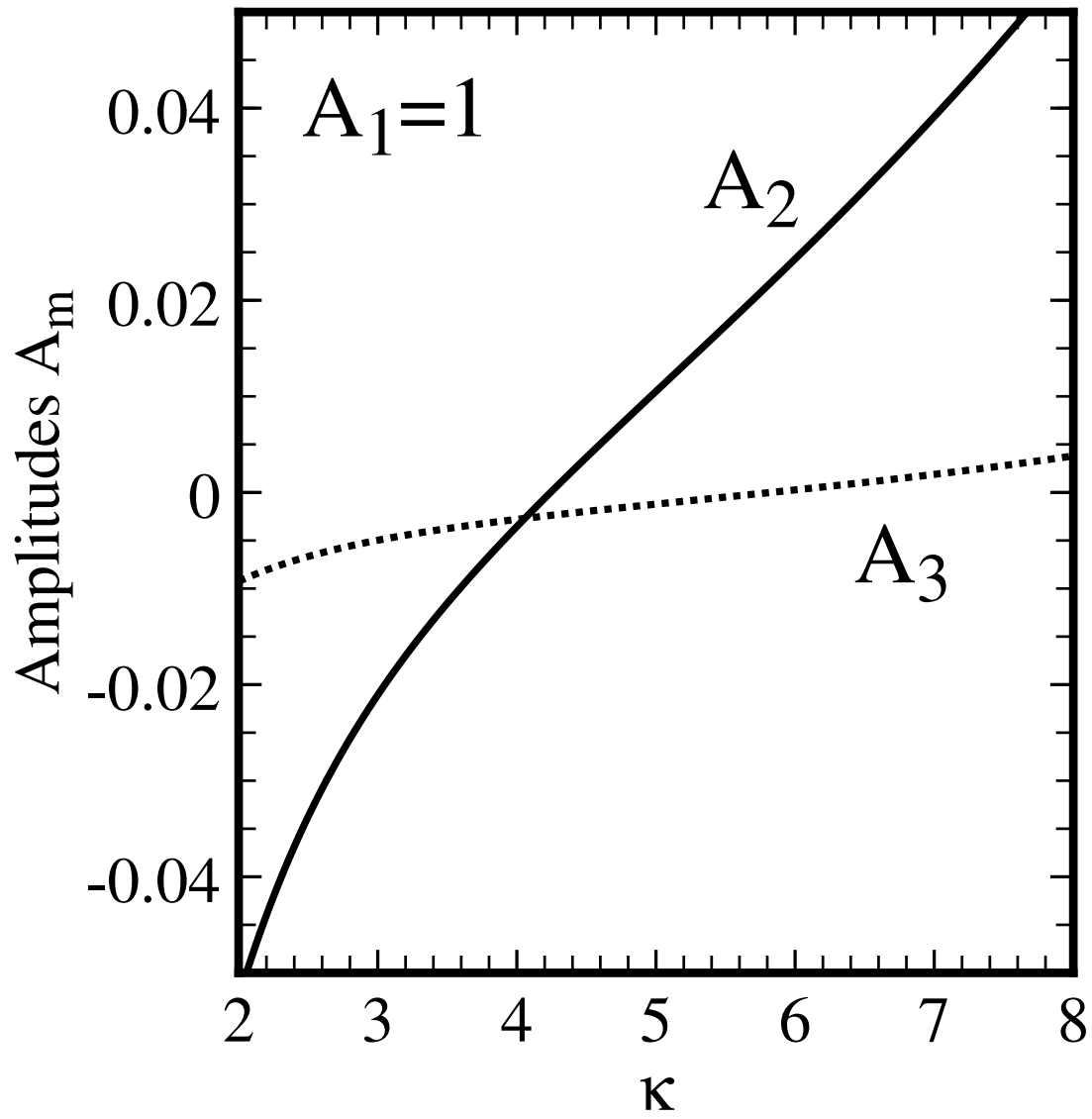FIG. 5. Q_{wire} and Q_{plate}

FIG. 6. Neutral Stability Boundary

FIG. 7. Relative amplitudes of the first three modes of the velocity field in the "wire" case.
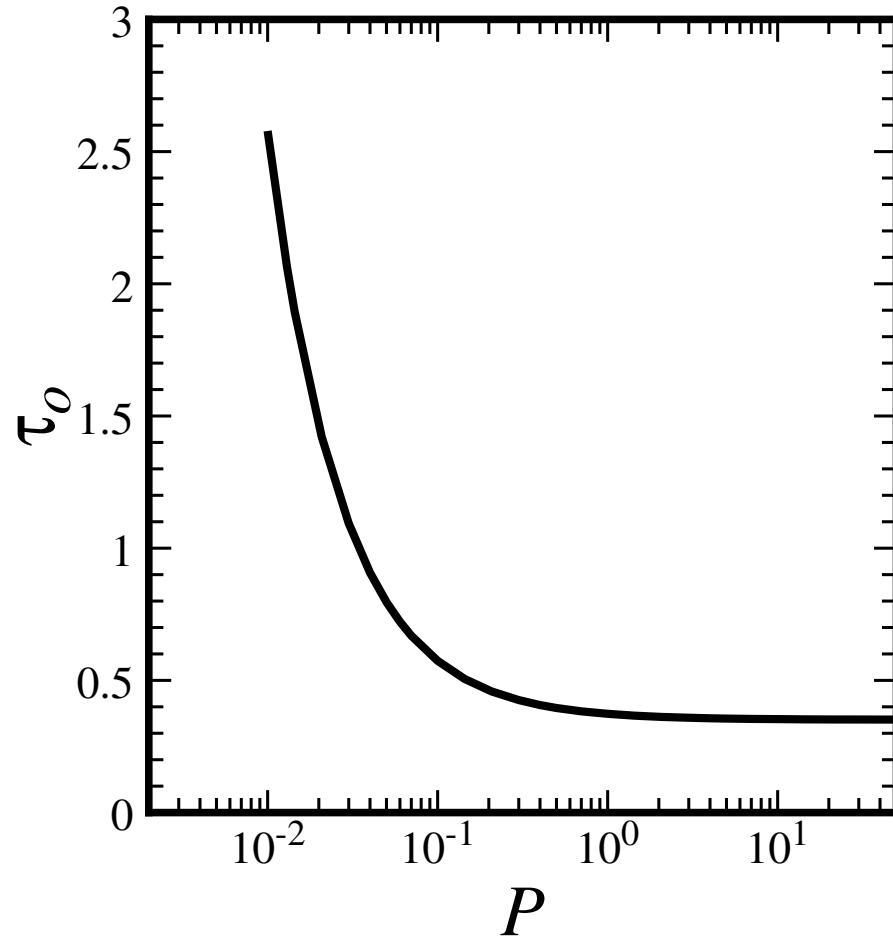
FIG. 8. Linear Growth Rate as function of the Prandtl-like number for the "wire" case.
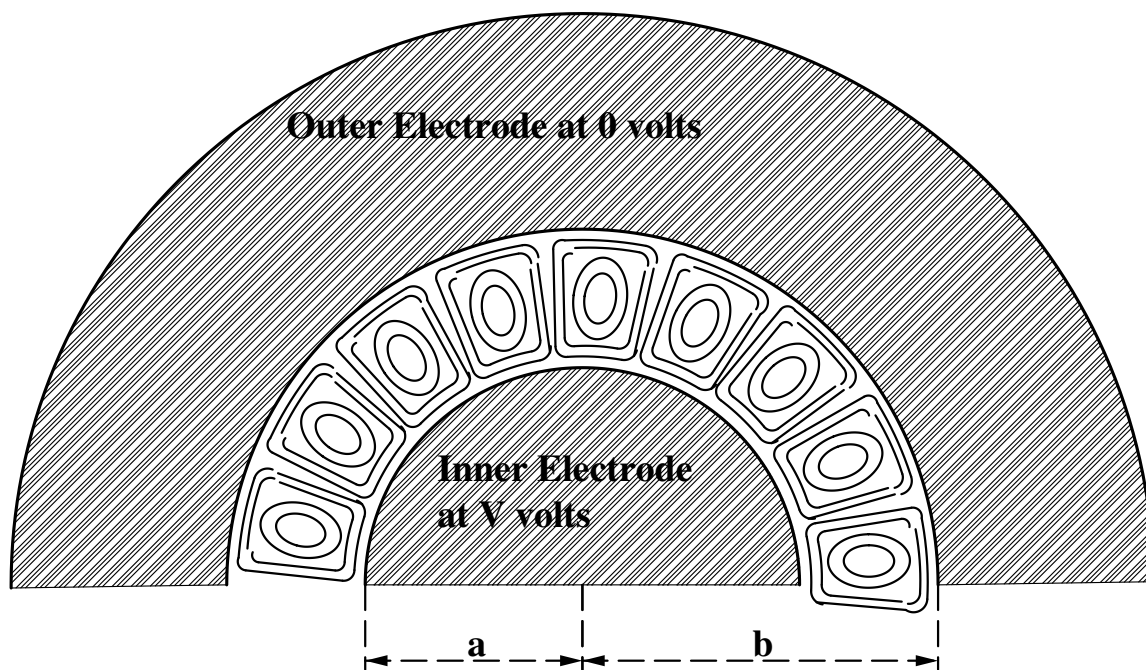
FIG. 9. Schematic of an Annular film.

TABLES

TABLE I. Quantities calculated from the neutral curve.

electrode geometry	wires	plates
critical wavenumber, κ_c	4.744	4.223
critical control parameter, $\mathcal{R}_c$	76.77	91.84
correlation length, ξ_0	0.2843	0.2975

TABLE II. The linear growth rate, $\tau_0{}^{-1}$.

$\mathcal{P}$ parameter	τ_0 for wire electrodes	τ_0 for plate electrodes
0.01	2.578	2.742
0.03	1.094	1.162
0.10	0.574	0.609
0.30	0.426	0.451
1.00	0.374	0.395
10.00	0.354	0.374
∞	0.351	0.372